REACTION RATE MEASUREMENT OF $C_2H_5OH \rightarrow C_2H_4+H_2O$ DURING ETHANOL PYROLYSIS USING H_2O TIME HISTORY MEASUREMENTS BEHIND REFLECTED SHOCK WAVES

A Thesis

by

LAURA TATIANA PINZON CORREA

Submitted to the Office of Graduate and Professional Studies of
Texas A&M University
in partial fulfillment of the requirements for the degree of

MASTER OF SCIENCE

Chair of Committee, Eric L. Petersen
Committee Members, Waruna Kulatilaka
Chad Mashuga
Head of Department, Andreas A. Polycarpou

August 2018

Major Subject: Mechanical Engineering

ABSTRACT

The thermal decomposition of ethanol has been studied under pyrolytic conditions behind reflected shock waves in the 1250 to 1677 K temperature range, at an average pressure of 1.31 atm for a mixture highly diluted in Ar. A laser absorption technique was utilized to measure H_2O time-histories, and the detailed kinetics mechanism (Aramco2.0) was selected among various models from the literature based on its *a priori* agreement with the experimental data in the present study. Sensitivity and rate-of-production analyses were performed and showed that the $C_2H_5OH \rightarrow C_2H_4+H_2O$ (R1) decomposition pathway is almost the sole reaction contributing to H_2O formation at the early times under the present conditions, allowing an *a priori* direct measurement of its rate coefficient k_1. The rate coefficient was determined to be defined as the Arrhenius equation k_1 (s^{-1}) = 3.37×10^{11} exp (-27174 K/T), which is in very good agreement with (Kiecherer et al., *Proc. Combust. Inst.* 35 (2015) 465-472) where k_1 was also directly determined under similar conditions. Secondary chemical reactions taking place in the thermal decomposition have very low influence in the H_2O formation during the time-frame selected, leading to an uncertainty for k_1 of approximately 20%. The full H_2O time histories under oxidation conditions at 0.5, 1.0 and 2.0 equivalence ratios were measured to validate the full ethanol detailed kinetics mechanism. The rate coefficient found in this study was utilized in the Aramco 2.0 model and was compared against experimental data and well-known detailed kinetic mechanisms.

ACKNOWLEDGMENTS

I would like to thank Dr. Eric L. Petersen, for giving me the opportunity to join his lab and work on this exciting research project, for his incredible support and guidance throughout the course of my master's degree, and for offering me high-quality instruction in courses like gas dynamics and combustion science.

My sincerest gratitude goes to my colleague and friend, Dr. Olivier Mathieu, for teaching me how to run the shock tube, for providing constant guidance on my research, and helping me to run all the experiments at the shock-tube laboratory. Furthermore, I would like to thank him for teaching me how to run and analyze the data on the Chemkin software program. Thank you for believing in my skills and your entire support.

I would also like to thank Clayton Mulvihill for his work on the laser diagnostic part of this research. Finally, a sincere thank you to all of my remaining lab colleagues for their support.

CONTRIBUTORS AND FUNDING SOURCES

Contributors

This work was supervised by a thesis committee consisting of Professor Eric L. Petersen (advisor) of the Department of Mechanical Engineering.

All work for the thesis was completed by the student, in collaboration with Dr. Olivier Mathieu, member of the Petersen research group of the Department of Mechanical Engineering. The laser diagnostic was done by Clayton Mulvihill, Ph.D. student of Mechanical Engineering and member of the Petersen research group.

Funding Sources

Funding for this work was provided primarily from the U.S. Department of Energy within the Co-Optima project grant DE-EE0007981 through a subcontract with the Louisiana State University (LSU), with Dr. Ingmar Schoegl as the Principal Investigator at LSU.

Additional funding came from the National Science Foundation under award number CBET-1706825.

NOMENCLATURE

ST	Shock Tube
φ	Equivalence Ratio
k_1	Rate Coefficient
τ_{ign}	Ignition Delay Time
MT	Mixing Tank
P	Static Pressure
t	Time
T	Static Temperature
ROP	Rate-of-Production
RMS	Root mean square roughness
I	Transmitted intensity
I_0	Incident intensity
k_v	Absorption coefficient ($cm^{-1}atm^{-1}$)
P_{abs}	Partial pressure of water
L	Path length
TDL	Tunable diode laser
$S(T)$	Linestrength
$\phi(\bar{\nu}-\bar{\nu}_0)$	Lineshape
ϑ_{ki}	Stoichiometric coefficient for the reactions
q_i	Rate of progress of the I gas-phase reaction

Subscripts

1	Initial condition of the driven section of the shock tube at t = 0
2	Condition behind the incident shock wave
3	Condition in the driver section behind the contact surface and the expansion wave
4	Initial condition of the driver section at t = 0
5	Condition behind the reflected shock wave in the driven section

TABLE OF CONTENTS

Page

LIST OF TABLES

Page

LIST OF FIGURES

Page

1. INTRODUCTION

To reduce CO_2 emissions responsible for global warming and/or oil dependency, many countries rely more and more on the use of biofuels in the transportation sector. According to the International Energy Agency [1], the use of biofuels will rise from 1.3 million barrels of oil equivalent per day (mboe/d) in 2010 to 4.5 mboe/d in 2035. Among these biofuels, ethanol, C_2H_5OH, is the most widely used [2]. Still according to the International Energy Agency, ethanol production will increase from 1 mboe/d in 2010 to 3.4 mboe/d in 2035. Nowadays, ethanol is mixed up to 20% in gasoline in the U.S., 85% in Europe (E85), and it is even used pure in Brazil, with minor engine modifications [3].

The large usage of ethanol as a transportation fuel can be explained by the fact that it is easily produced from renewable sources. Ethanol is primarily produced from the fermentation of sugar and starches. One can mention notably sugar cane in Brazil and (mostly) corn in the USA (these two countries being the 2 largest ethanol producers [4]). Note that intensive research is currently being carried out to produce ethanol from other renewable sources. For instance, lignocellulose is currently considered [5,6] as it does not compete with food production, like corn. A more extensive discussion on the sustainability of ethanol production can be found in the paper of Sarathy et al. [4].

From a transportation fuel standpoint, the physical and combustion properties of ethanol are very suitable for spark ignition (SI) engines. This suitability has been known for more than 85 years, as visible in the pioneer work of Ricardo [7]. Ethanol is an octane and a sensitivity (RON-MON

value) enhancer, which helps in preventing engine knock [8]. Fuels that are not prone to auto-ignition are highly desirable for SI engines since they allow advancing of the spark timing and increased engine efficiency [4]. In addition, when mixed with gasoline, ethanol increases the flame propagation in a SI engine [9], which enhances combustion stability and improves engine efficiency. Finally, the addition of ethanol has been shown to decrease soot formation [10].

These benefits of ethanol as a fuel or a fuel additive triggered various research studies to understand the details of its combustion chemistry. Notably, important combustion parameters for engine combustion such as ignition delay time [11-19] and laminar flame speed [20-32] were investigated over the past few years. Fundamental speciation data have also been taken in a large variety of apparatuses such as flow reactors [33-39], jet-stirred reactors [40-42], shock tubes [43], micro-flow reactors [44], and various kind of flames [45-50] to further refine models. In addition, an extensive amount of work has focused on a few specific reactions in experimental and theoretical studies [38,51-56].

There is a consensus in the literature that the reactivity of ethanol is essentially initiated by the following endothermic decomposition pathways [38,51-57]:

$$C_2H_5OH \rightarrow C_2H_4+H_2O \quad (R1)$$

$$C_2H_5OH \rightarrow CH_3+CH_2OH \quad (R2)$$

$$C_2H_5OH \rightarrow C_2H_5+OH \quad (R3)$$

It is also established that R1 is the dominant reaction pathway over a large range of conditions [52,54,56]. The rates of the reactions R1-R3 have been studied experimentally in shock tubes [54-58], but it is worth mentioning that these experimental studies only inferred the rate coefficient of k_1, whereas k_1 was *a priori* measured directly in the study of Kiecherer et al. [56] only. In this latest study, the concentration-time profiles of several species were recorded using time-of-flight-mass spectrometry and they determined that the H_2O concentration is very weakly influenced by reactions other than k_1 at early times. By using the early times of the slope of the H_2O concentration time history profile, they were able to determine k_1 directly. The reaction rate determined experimentally was in very good agreement with the value they calculated using RRKM theory, and it is in relatively good agreement with other experimental data measured under similar conditions, as can be seen in Fig. 1. However, while this recent measurement was *a priori* direct, the error margin for k_1 was estimated to be ± 40% due to the scatter in the data induced by their measurement technique.

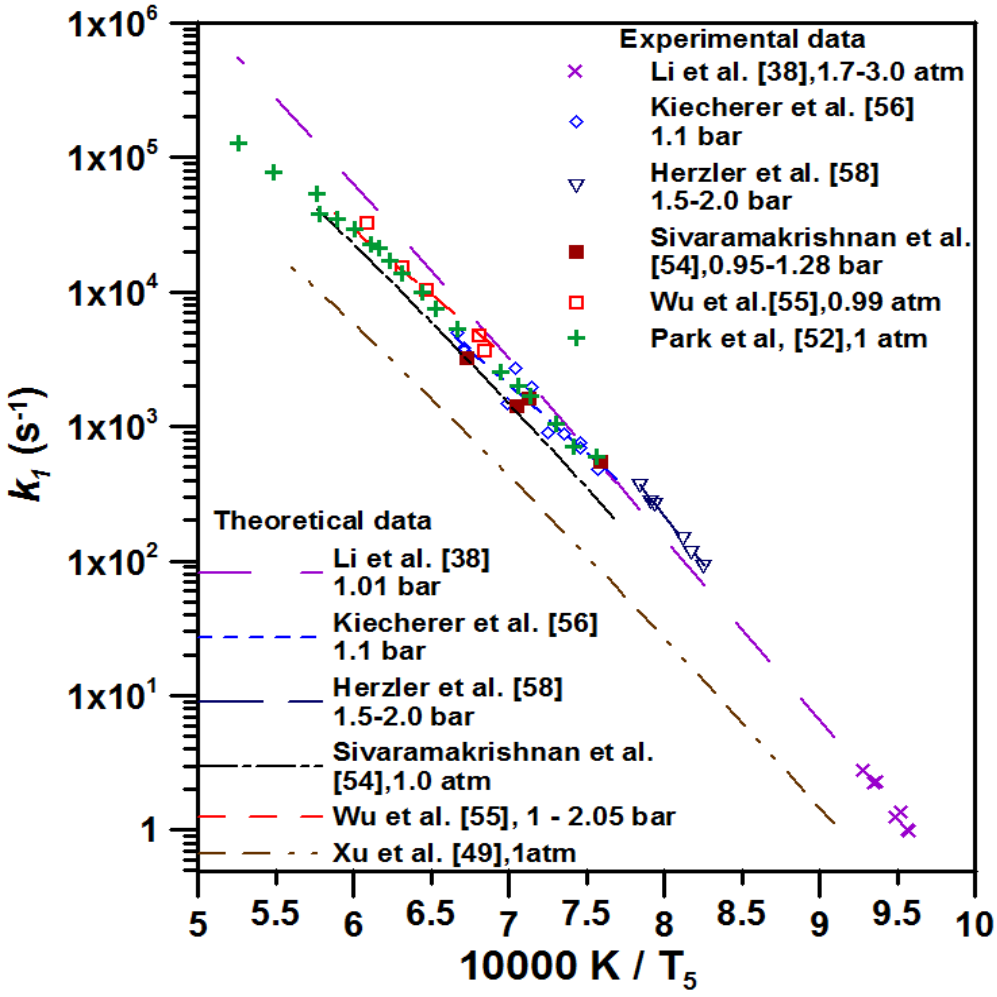

Figure 1: Arrhenius plot of experimental and theoretical studies for k_1. Symbols represent experimental data and lines the theoretical calculations.

Due to the large importance of R1 in ethanol combustion chemistry, a direct measurement of its rate coefficient k_1 with a lower error margin and over a larger range of temperatures would be beneficial to further refine detailed kinetics models. To this end, H_2O time-histories during ethanol pyrolysis were measured behind reflected shock waves using laser absorption in the present study. Such a technique presents a signal/noise that is advantageous compared to the scattered data

obtained in [56]. In addition, the time resolution of the laser measurement and sampling rate of the digital oscilloscope used in the author's laboratory at Texas A&M University (1 MHz) are 1.2 times higher than the technique used by Kiecherer and coworkers. It is therefore expected that the present experimental setup allows for measuring k_1 with a lower error margin. In addition to using the shorter times of the H_2O histories to determine the rate coefficient k_1, the profiles are also useful for validating complete chemical kinetics mechanisms over the entire duration of the experiment. To help further in validating the models, in addition to the pyrolysis experiments mentioned above, the H_2O profiles for mixtures of ethanol at three equivalence ratios (0.5, 1.0, and 2.0) were also studied. Models were similarly assessed against these oxidation data, and a modern mechanism updated with the new reaction rate for k_1 measured with the pyrolysis data will also be used.

First in this study is a description of the shock-tube and laser-absorption diagnostic used to measure H_2O time-histories from ethanol pyrolysis. The methodology employed to perform an *a priori* direct measurement of k_1 is then detailed, and a rate coefficient for k_1 is measured from the new experiments. This rate coefficient is then discussed and compared to literature values. After this discussion, the oxidation data are presented and compared, along with the pyrolysis data, with detailed kinetics mechanisms. Finally, a numerical chemical analysis is conducted to explain and understand the results presented herein.

2. EXPERIMENTAL APPARATUS AND NUMERICAL TOOLS

2.1 Shock Tube

A single-diaphragm, stainless-steel shock tube was used to measure water time-history profiles behind reflected shock waves by using the laser absorption technique for mixtures of ethanol highly diluted in Ar. The driven section of the shock tube is 16.20-cm i.d., 6.78-m long (304 stainless steel, with a 1.27-cm wall thickness), whereas the driver section is 7.62-cm i.d., 3.00-m long (SAE 4340 forged steel, with a 1.27-cm wall thickness). A schematic of the shock-tube setup is provided in Fig. 2.

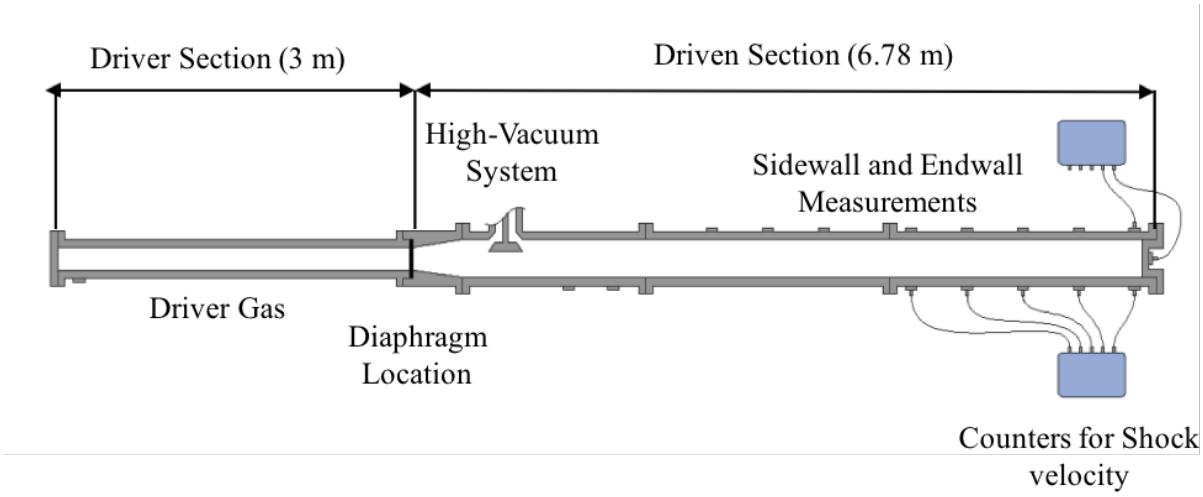

Figure 2: Schematic of stainless steel shock tube, displaying main sections.

More details on the shock tube are available in J. E. Vivanco [71]. The inside of the driven section was polished to a surface finish of 1 μm root mean square roughness (RMS) to minimize boundary layer growth. Shock wave speed was measured using five PCB P113A22 piezoelectric pressure

transducers alongside the driven section. These transducers were mounted flush with the inner surface, with a well-known spacing between them. The incident shock wave velocities were determined using signals delivered by these transducers and four Fluke PM-6666 timer/counter boxes. The incident wave speed was determined using a curve fit of these velocities and extrapolated to the endwall location.

Post reflected-shock conditions were obtained using this extrapolated wave speed in conjunction with one-dimensional shock relations and the initial conditions at the test region. This method was proven to maintain the uncertainty on the temperature determination behind reflected shock waves (T_5) below 10-15 K [59]. Test pressure was monitored by a Kistler 603 B1 transducer located at the sidewall, in the same plane as the CaF_2 observation windows, located 16 mm from the endwall. Non-ideal boundary layer effects measured by the change in pressure (dP/dt) behind the reflected shock wave were determined to be less than 2% per ms for all experiments. Due to the dilution level used, these non-ideal effects are essentially due to the facility and can be associated with the growth of boundary layers, not to the heat released by the reactivity of the mixture. The corresponding increase in temperature for these dP/dt levels would be less than 10-15 K for the longest test times reported here and therefore does not have a noticeable impact on the results herein.

Experiments were performed at around 1.3 atm, under pyrolysis and for three equivalence ratios (ϕ) of 0.5, 1.0, and 2.0. Polycarbonate diaphragms, 0.25-mm thickness, were used, and a cross-shaped cutter was employed to facilitate breakage of the diaphragm and prevent diaphragm fragments from tearing off. Helium was used as the driver gas during this study, but a small fraction

of air was introduced in the driver for the lowest temperatures investigated herein, to extend the test time.

Prior to every run, the driven section was vacuumed down to 2×10^{-5} Torr or better using a roughing pump and an Agilent Turbo-V1001 turbo molecular pump, backed by an Agilent DS402 pump. The pumping time between experiments was minimized using a pneumatically driven poppet valve matching the inside diameter of the driven section and allowing for a passage of 12.7-cm diameter between the vacuum section and the driven tube. The pressure is measured using two MKS Baratron model 626A capacitance manometers (0-10 Torr and 0-1000 Torr). Test mixtures were prepared manometrically in a mixing tank of 1.52-m length made from stainless steel tubing with a 15.24-cm ID. The pressure in the mixing tanks was measured using a Setra GCT-225 pressure transducer (0-17 atm). The mixing tank is connected to the vacuum system and can be pumped down to pressures below 1×10^{-6} Torr. The gases (O_2 and Ar) were both ultra-high purity (99.999%) and purchased from Praxair. Ethanol (99.5%) was purchased from Sigma Aldrich. The ethanol was introduced first into the mixing tank via a vial connected to the shock-tube manifold. The liquid fuel was degassed several times prior to being introduced into the mixing tank, and the vapor pressure of ethanol introduced into the tank was kept at 50% or less of the saturating vapor pressure. The gases were passed through a perforated stinger traversing the center of the mixing tank to allow for rapid, turbulent mixing. To further ensure homogeneity through diffusion processes, mixtures were allowed to rest for at least 45 min prior to making the first run. No difference in the results was observed for longer mixing times. Conditions investigated during this study are provided in Table 1.

Table 1: Conditions investigated for pyrolysis and oxidation of ethanol.

% C_2H_5OH	% O_2	% Ar	Equiv. ratio	Measurement	Pressure (atm)	Temperature (K)
0.75	0	99.25	∞	H_2O	1.23 – 1.41	1250 - 1677
0.107	0.643	99.25	0.5	H_2O	1.34 – 1.43	1298 - 1513
0.1875	0.5625	99.25	1.0		1.34 – 1.42	1313 - 1486
0.30	0.45	99.25	2.0		1.31 – 1.38	1426 - 1613

All of the data signals were recorded through a 14-bit GageScope digital oscilloscope with sampling rates of 1 MHz or greater per channel. All of the simulations within this study were performed using the Chemkin Pro package from Reaction Design [60]. The computation was made using the Closed Homogeneous Reactor model, along with the Constrain Volume and Solve Energy Equation problem type. Specific details on the mechanisms employed to compare with the data are provided later.

2.2 H_2O Laser Diagnostic

To study the formation of water during ethanol thermal decomposition and combustion, a laser absorption technique was used. The laser light was generated at 7203.890 cm^{-1} (1388.139 nm) by a Toptica Photonics DL100L tunable diode laser with a linewidth of ~1 MHz to a to probe the $5_{5,1}\leftarrow5_{5,0}$ transition of H_2O in the fundamental $\nu_1+\nu_3$ band. The wavelength of the laser was monitored by a Burleigh WA-1000 wavemeter with an uncertainty of ±0.0005 nm during the course of an experiment and was controlled by a temperature and current controller (Toptica Photonics DC110). Typical operating conditions for the laser were 20.0°C and 98 mA. The

incident (I_0) and transmitted (I) laser intensities were measured using a pair of Newport 2317NF photodetectors, allowing for the transient water concentration within the shock tube to be calculated using the Beer-Lambert relation, $I/I_0=\exp(-k_v P_{abs} L)$ (with k_v the absorption coefficient ($cm^{-1}atm^{-1}$), P_{abs} the partial pressure of water (atm), and L the path length (16.2 cm, corresponding to the inner diameter of the driven section). The absorption coefficient kν is the product of the lineshape and linestrength. A schematic of the optical setup is visible in Fig. 3.

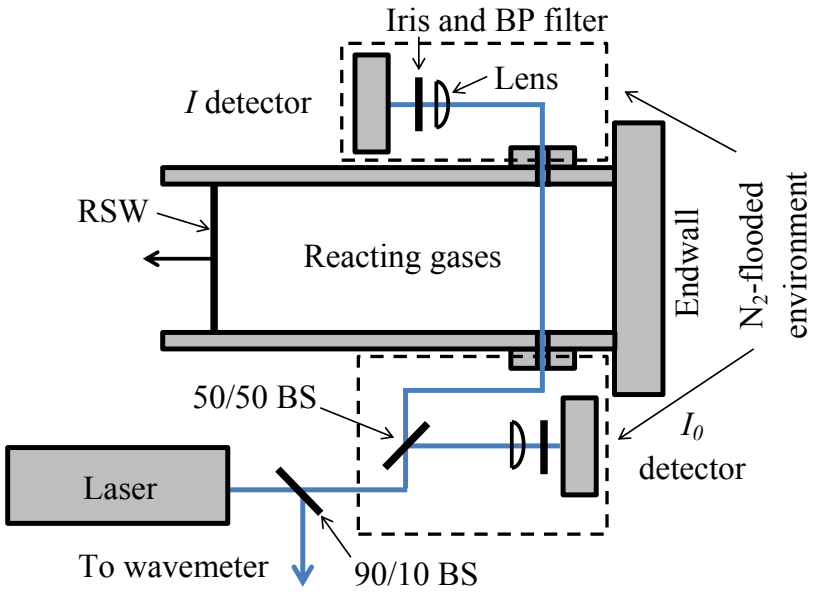

Figure 3: Schematic of the laser diagnostic used during this study.

The detector signals were sampled via a digital oscilloscope at 1 MHz using common-mode rejection through a low-noise differential preamplifier (Stanford Research Systems model 560). Both detectors were fitted with a bandpass filter centered at 1384 nm with a full width at half

maximum of 10 nm. The measured portion of the laser beam path was purged with N_2 to avoid any interference with water from the ambient. The laser beam path was placed into an in-house made Lexan box equipped with a hygrometer, as can be seen in Fig. 4.

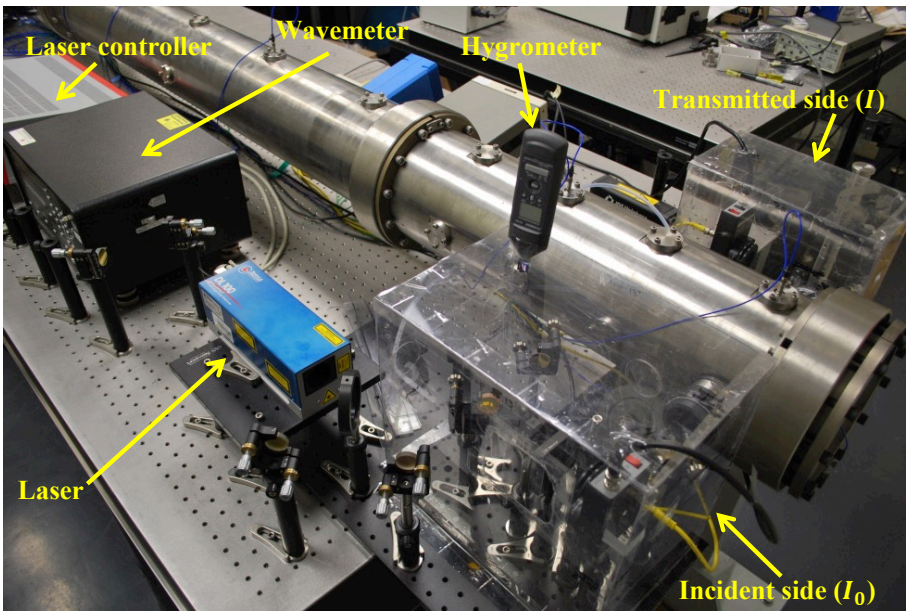

Figure 4: Shock-tube laser diagnostic setup.

The reactions taking place in these experiments caused noticeable temperature changes over the 2-3 milliseconds of test time. The computed temperature was increased by up to 130 K for the stoichiometric condition, and decreased by up to 50 K for the pyrolysis case, according to the Aramco 2.0 model [69]. A correction was therefore applied to the absorption coefficient for each measurement since k_v is a strong function of temperature ($k_v=S(T)\phi(\bar{\nu}-\bar{\nu}_0)$). To quantify the corrections applied, it is worth noting that this temperature decrease caused a ~7% rise in k_v. Linestrength $S(T)$ is obtained from the HITRAN spectroscopic database [61] and the lineshape $\phi(\bar{\nu}-\bar{\nu}_0)$ is given by the Voigt profile, as approximated by the expression from Whiting [62]. The

Voigt profile is the convolution of thermal and collisional broadening effects. Lineshapes were calculated according to Nagali et al. [63]. These broadening effects are functions of temperature and species concentrations. The simulated temperature rise was therefore used to calculate a transient absorption coefficient profile, which was then applied to the raw data to obtain a water time-history, as previously described in Mathieu et al. [64]. Uncertainties in the measurements are essentially due to the uncertainty in the temperature determination. The detection level ranged from 0.9 to 1.9% absorption, and the estimated accuracy on water concentration is between 5 and 6%. The dilution level used herein (99.25% Ar) was selected to have a good balance between the detection level and the exothermicity. Blank runs with Ar were performed between experiments to ensure no residual amount of water could be detected.

2.3 Sensitivity Analysis

During this study, the sensitivity analysis from Chemkin Pro [60] was used to determine the important reactions driving the formation of H_2O under our experimental conditions. The sensitivity analysis consists of the determination of σ, the sensitivity coefficient for every single reaction of the detailed kinetics model used for computational simulations. In Chemkin Pro, the sensitivity analysis considers the first-order sensitivity coefficients of the H_2O mole fraction with respect to the reaction rate coefficients [65]. The calculation is done for every single reaction by the software corresponds to the partial derivative of the natural logarithm of the H_2O concentration with respect to the natural logarithm of the reaction rate of the considered reaction.

$$\frac{\partial \ln[H_2O]}{\partial \ln [K_i]}$$

With [H_2O] the mole fraction of H_2O, and *Ki* is the rate constant of the considered reaction *i*. More details about the sensitivity analysis are available in the Theory Manual, accessible online [65].

2.4 Rate of Production Analysis- ROP

After the sensitivity analysis, the rate-of-production (ROP) analysis was used to understand better the chemistry behind the formation of water during our experiments. As indicated in the Chemkin Pro manual [65], the rate-of-production analysis determines the contribution of each reaction to the net production or destruction rates of a species (water in the present case).

The modeling of the shock-tube results was performed under the assumption of a 0-D homogeneous system. For such system, the molar production of a species per unit volume, P_k, is given by:

$$P_k = \sum_{i=1}^{I} \vartheta_{ki} q_i$$

Where ϑ_{ki} is the stoichiometric coefficient for the reactions and q_i the rate of progress of the I gas-phase reaction. The contribution to the ROP of species k from reaction i is therefore $C_{ki} = \vartheta_{ki} q_i$. The reactor model computes normalized values of the reaction contributions to the species production and destruction rates. The normalized production-contributions for gas-phase reactions are visible in the Chemkin manual [65]. Note that during our simulations, the above calculations were performed at every time step, set to 1 µs, to match the data acquisition frequency of the experimental set-up.

3. REACTION RATE DETERMINATION METHOD

As shown later, and in agreement with Kierecher et al. [56], the selection of the initial ethanol mechanism is not very important for the pure determination of k_1 because R1 is almost not influenced by secondary reactions at early times. However, since many other reactions are involved in H_2O formation during the time-frame of the present experiments, it is important to select the most-accurate mechanism over the full time scale of the experimental data, so it can be used as a base to refine the ethanol chemistry and estimate the influence of the secondary reactions on the determination of k_1. To this end, the H_2O profiles obtained experimentally during this study were compared to a variety of detailed kinetics mechanism from the literature. Namely, the classical model from Marinov [51]; the ethanol mechanisms from Cancino et al. [15] (referred to as Cancino hereafter); Leplat et al. (Leplat) [42]; the gasoline surrogate model from Mehl et al. [66] (LLNL); and the base hydrocarbon mechanisms from Politecnico di Milano (Ranzi et al. [67,68], (CRECK)), and from National University of Ireland Galway (Aramco2.0) [69].

Some representative H_2O time-history profiles and their comparisons with the aforementioned detailed kinetics models are visible in Fig. 5. As can be seen, the Marinov, Leplat, and Aramco2.0 mechanisms offer good predictions overall, under the current experimental conditions, whereas the Cancino, LLNL, and CRECK models demonstrate large discrepancies with the present data. Among the most-accurate models, Aramco2.0 provides better predictions at earlier and, especially, later times, where both Leplat and Marinov over-estimate the amount of water. The Aramco2.0 was therefore selected as the base mechanism for this study. Note that more experimental profiles are compared with models in the Appendix section.

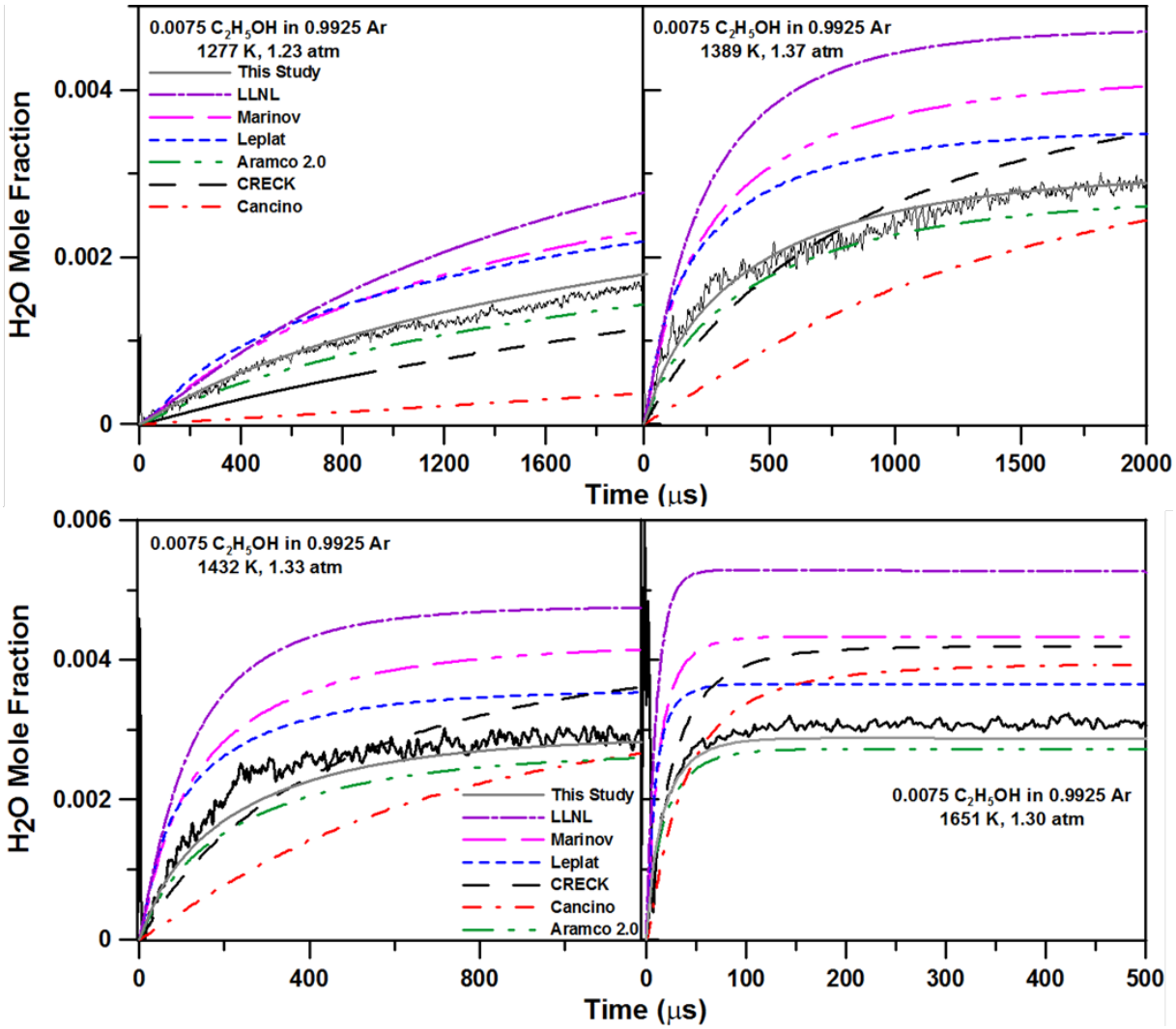

Figure 5: H_2O time-history profiles for the pyrolysis of 0.0075 C_2H_5OH in 0.9925 Ar and comparison with detailed kinetics models from the literature.

The Aramco2.0 mechanism was then used to perform sensitivity and rate-of-production (ROP) analyses for H_2O. Figure 6 shows the results of the sensitivity analyses for the highest and lowest temperatures investigated herein. The rate-of-production analyses at these temperatures confirmed

the domination of R1 for water formation under the present experimental conditions, and they are visible in Figure 7. These analyses show that R1 is, by far, the most sensitive reaction under the present conditions, especially during the earlier times (i.e. the first 50 μs at higher temperature to the first 100 μs at lower temperature). The ROP analysis also confirms that H_2O and C_2H_4 are, by a large margin, the main products of the decomposition of ethanol at the beginning. The endothermic reaction R1, $C_2H_5OH \leftrightarrows C_2H_4+H_2O$, is therefore the dominant pathway for H_2O production, which is in agreement with Kiecherer et al [56]. Moreover, the sensitivity analysis shows that, among the top five most-sensitive reactions, none is forming water directly after R1. The analysis at 1250 K, for instance, shows the most-sensitive reactions to be in order of importance:

$$C_2H_5OH \leftrightarrows C_2H_4+H_2O \quad (R1)$$

$$C_2H_4+OH \leftrightarrows C_2H_3OH+H \quad (R4)$$

$$C_2H_5OH+H \leftrightarrows SC_2H_4OH+H_2 \quad (R5)$$

$$C_2H_5OH \leftrightarrows CH_3+CH_2OH \quad (R2)$$

$$C_2H_3OH \leftrightarrows CH_3CHO \quad (R6)$$

Whereas the sensitivity analysis at 1677 K leads to the following results:

$$C_2H_5OH \leftrightarrows C_2H_4+H_2O \quad (R1)$$

$$C_2H_5OH \leftrightarrows CH_3+CH_2OH \quad (R2)$$

$$C_2H_5OH+H \leftrightarrows PC_2H_4OH+H_2 \quad (R7)$$

$$C_2H_4+OH \leftrightarrows PC_2H_4OH \quad (R8)$$

$$C_2H_5OH+H \leftrightarrows SC_2H_4OH+H_2 \quad (R5)$$

Despite the fact that both sensitivity and ROP analyses present some differences at the extremes of the temperature range investigated, the reaction $C_2H_5OH \leftrightarrows C_2H_4+H_2O$ (R1) has the strongest influence, leading one to believe that the secondary reactions have very low to no influence in the H_2O formation at early times. This point is further detailed later during the error uncertainty analysis.

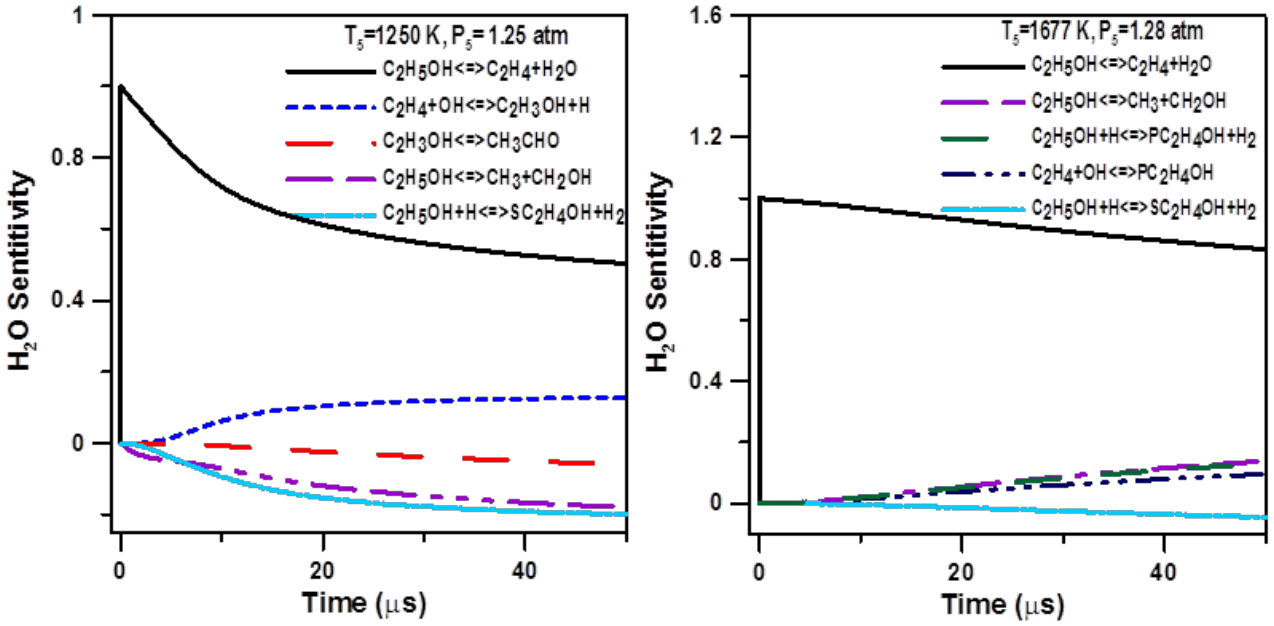

Figure 6: Sensitivity analysis on H_2O at 1250 and 1677 K with the Aramco2.0 mechanism for a mixture of 0.0075 C_2H_5OH in 0.9925 Ar.

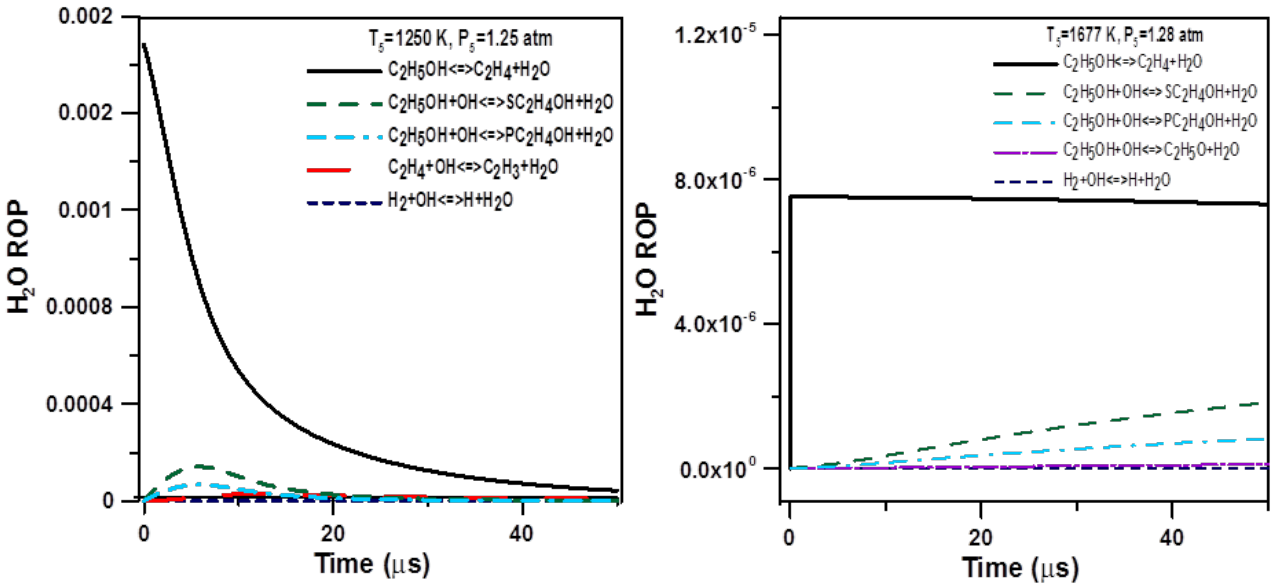

Figure 7: Rate of Production (ROP) analyses for H_2O at 1250 and 1677 K with the Aramco2.0 mechanism for a mixture of 0.0075 C_2H_5OH in 0.9925 Ar.

Once it has been confirmed that k_1 dominates the formation of H_2O at early times, a value for its rate constant was manually assigned into the Aramco 2.0 model for each experiment through an iterative process until the best fits for the early times of the H_2O time histories were found. Some examples of the best fit assigned to the experimental profiles are visible in Fig. 8 and in the Appendix section. The value of the rate constant of k_1 determined to fit one experimental profile was then registered, and the same procedure was performed for each temperature and pressure condition investigated herein. The experimental rate constants for k_1 at each corresponding condition (pressure and temperature behind the reflected shock waves) are provided in the next section.

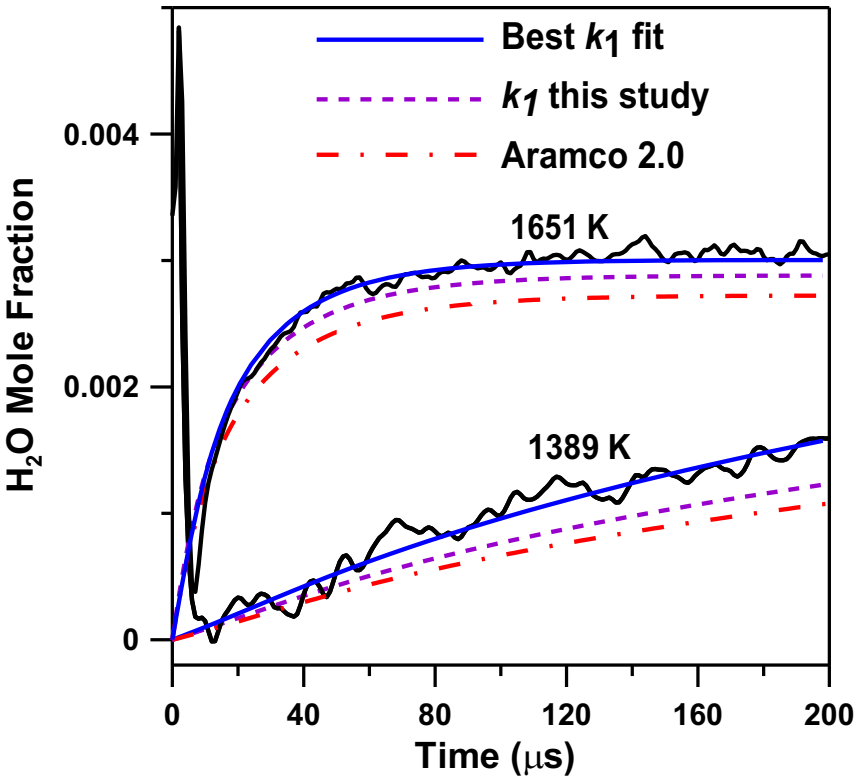

Figure 8: Best k_1 fit, measured R1 rate coefficient, and Aramco2.0 comparison.

4. RESULTS AND DISCUSSION

4.1 Rate Coefficient

Each value of the rate constant of k_1 was then plotted on an Arrhenius graph (Fig. 9), and the rate coefficient for the main reaction R1 was determined by finding the best fit to the rate constant graph. That fit was found to be exponential, and present a good R^2 value (0.99). Values of k_1 can be seen in Table 2. The rate coefficient determined from the results in Fig. 9 is:

$$k_1\ (s^{-1}) = 3.37\times10^{11}\exp(-27174\ K/T)$$

Table 2: Rate coefficients k_1 determined from the early times of the H_2O profiles and associated experimental conditions for a mixture constituted of 0.0075 C_2H_5OH / 0.9925.

T_5 (K)	P_5 (atm)	k_1 (s^{-1})
1250	1.25	105
1277	1.23	150
1294	1.31	315
1312	1.41	350
1321	1.33	400
1369	1.34	600
1389	1.33	1100
1389	1.37	1300
1392	1.32	1193
1432	1.33	2000
1453	1.28	3200
1487	1.29	3865
1521	1.31	6500
1538	1.28	9235
1579	1.28	10000
1651	1.30	20000
1677	1.28	26500

An example of the performance of the Aramco2.0 mechanism with the value of k_1 determined in the present study is visible in Figures 5 and 8. Note that predictions are still very good, if not better for longer test times (lower temperatures), despite the change in the rate coefficient of k_1. This result is due to the good selection of other important reaction rates past the first 100 μs within the Aramco2.0 model.

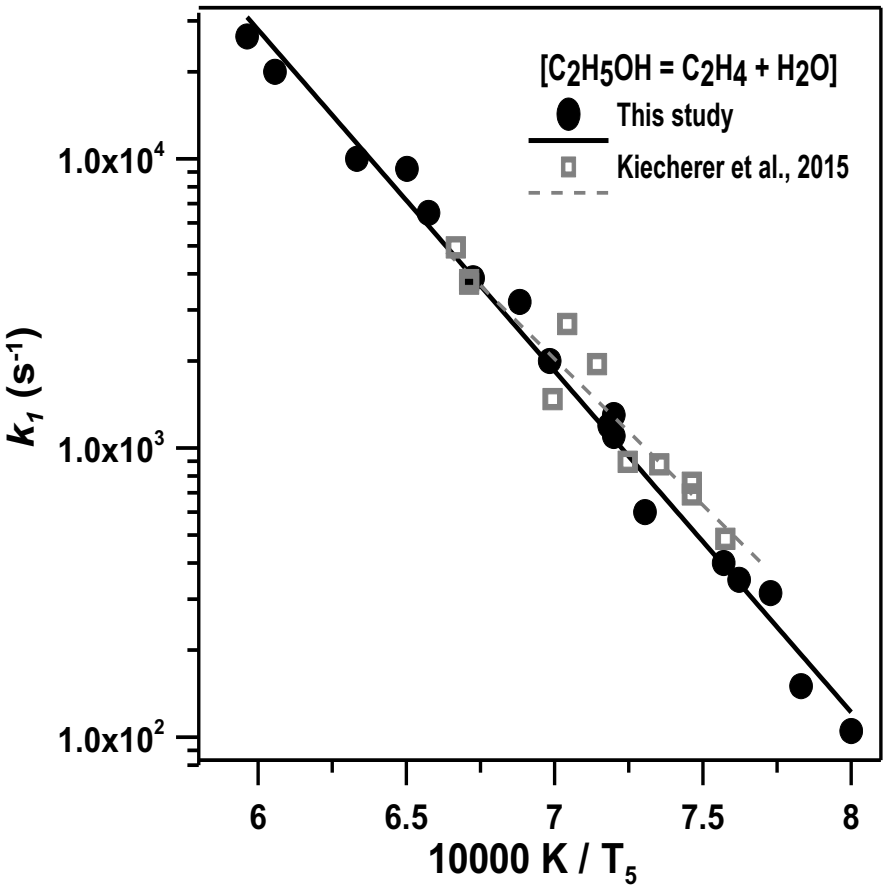

Figure 9: Arrhenius plot of the reaction rate coefficient k_1. Solid circles represent experimental data. Line represents exponential fit, k_1 rate coefficient.

4.2 Uncertainty of the Analysis

To estimate the uncertainty on the rate coefficient k_1 determined in the present study, different possible sources that could lead to errors in the measurements were investigated. As mentioned before, the temperature behind the reflected shock wave is estimated within 10 K, so the impact of a ±10 K variation in the initial temperature was investigated. As can be seen in Fig. 10a, a ±10 K variation at the lowest temperature investigated does change the predictions for times longer than 50 μs. At 100 μs, the ±10 K variation induces a change in the amount of water formed by ±20%. For the highest temperature investigated, where much more water is formed at 40 μs, the impact of this ±10 K variation is much lower, (2.4 and 2.7%). This small variation is not shown in Fig. 10b for readability purposes. Note that the use of a dilute, pyrolytic mixture does not induce an increase in pressure during the course of an experiment. However, non-ideal boundary-layer effects cannot be fully eliminated, and they often can be gauged by changes in pressure (dP/dt) behind the reflected shock wave. Thanks to the large diameter of the shock tube herein and the use of Ar as diluent, dP/dt was determined to be less than 2%/ms for all experiments. Since k_1 was determined within the first 40-100 μs (depending on the temperature) of the observation time (around 2000 μs with He as driver gas), these non-ideal boundary-layer effects were considered negligible in the present study.

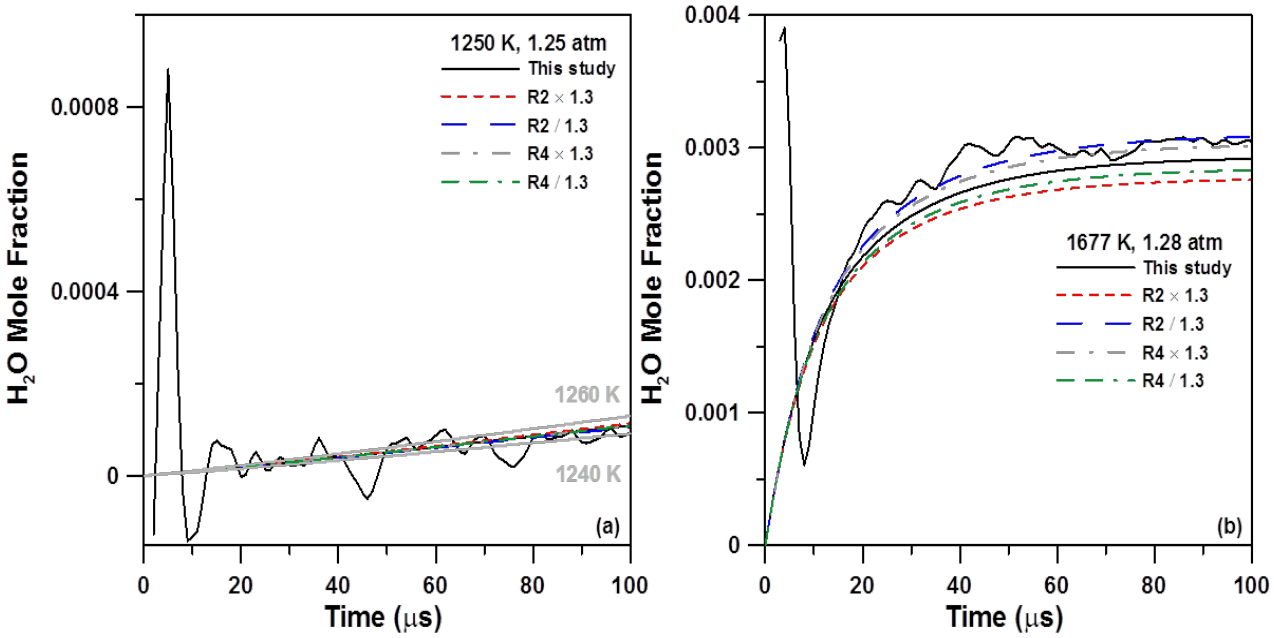

Figure 10: Influence on the water profiles of the uncertainty on the temperature and of the uncertainties in the rate coefficient of the most-sensitive reactions for water formation (after R1). Plot on the left (10.a) shows the uncertainty at 1250 K. Plot on the right (10.b) shows the uncertainty at 1677 K.

As seen in Fig. 6, the H_2O profile is sensitive to other reactions after a few tens of microseconds. The impact of these reactions (R2, R4-R8) on the computed water profile was investigated by individually changing their rate coefficients within their stated uncertainties. Two examples are given below, for R2 ($C_2H_5OH \leftrightarrows CH_3+CH_2OH$) and R4 ($C_2H_4+OH \leftrightarrows C_2H_3OH+H$), the two most-sensitive reactions for H_2O formation after R1, at the highest and lowest temperatures investigated herein, respectively (Fig. 6). The rate coefficient of R2 used in the Aramco2.0 model comes from the study of Sivaramakrishnan et al. [54]. The uncertainty in their rate coefficient of R2 is not clearly stated, but since experimental and theoretical results agreed well, a conservative 30% uncertainty on R2 was employed for the comparison calculation. The same uncertainty was applied for R4, originally coming from the study of Senosiain et al. [70].

As can be seen, for the lowest temperature investigated, (Fig. 10a), changing both reaction coefficients by a factor 1.3 does not modify the predictions of the Aramco2.0 model using the value of k_1 determined in the present study, for at least 100 μs. For the highest temperature investigated, Fig. 10b, changing both reactions by a factor 1.3 leads to a discernable effect in the model predictions after 20 μs. At 40 μs, varying R4 by a factor 1.3 induces a change in the amount of water formed by 3% or less. For R2, the most sensitive reaction after R1 at high temperature, such change in its reaction coefficient leads to changes in the predictions by less than 5%. Note that one can discern the effects of the changes in R2 and R4 (and in R5-R8) on the predicted H_2O profile for temperatures above 1500 K only. It can be concluded that the rate coefficient measurement of k_1 is free of the influence from other reactions over most of the temperature range investigated, and that influence is limited at high temperature.

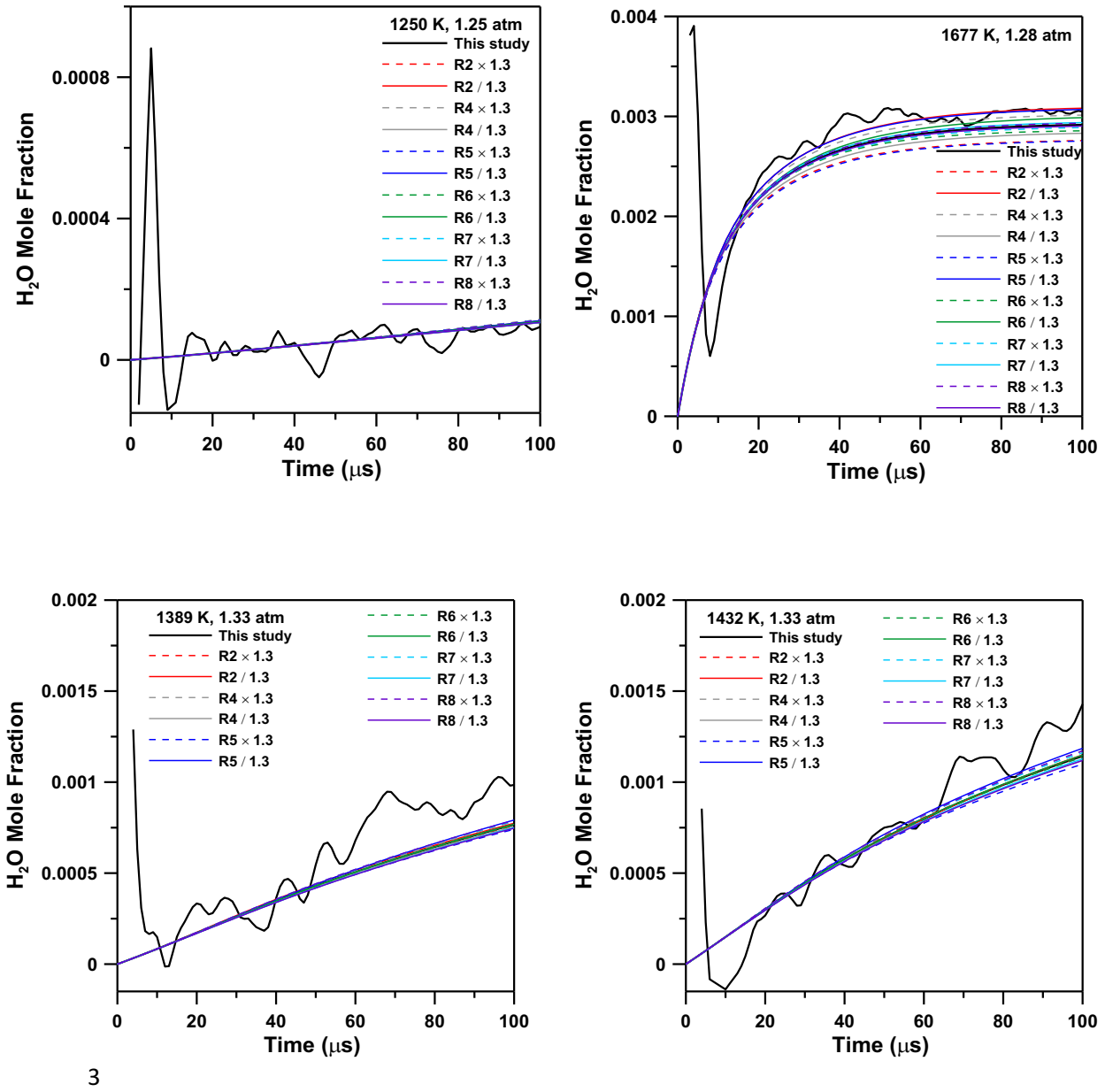

3

Figure 11: Influence on the water profiles of the uncertainties in the rate coefficient of the most-sensitive reactions for water formation (after R1).

The same procedure was applied to the less-sensitive reactions, R5-R8, and the results of these analyses are visible in Figure 11. Overall, the influence of these reactions is still negligible on the lower-temperature side, whereas the effect is visible, although to a lesser extent than R2, on the

higher-temperature side. The uncertainty in the present measurement of k_1 was therefore estimated to be between 20% at lower temperature (due to the ±10 K uncertainty) and less than 15% on the higher- temperature side (calculated by combining the individual uncertainties due to each rate in a sum-of-squares fashion). The overall, conservative uncertainty in the reaction rate coefficient of k_1 determined herein is therefore estimated at 20%.

4.3 Rate Coefficient Comparison with Literature Data

Data from the present study are compared to literature results in Fig. 12. As can be seen, the current study is in overall good agreement with Kiecherer et al. [56], Park et al. [52], and Wu et al. [55] which all have been obtained under similar pressure conditions. Good agreement was also reached with the data of Sivaramakrishnan et al. [54] for the few data points obtained at around 1 atm. In more detail, while the present data agree very well at high temperature with Kiecherer et al. [56] and Park et al. [52] , some discrepancy can be observed for lower temperatures. For example, for the lowest temperature investigated in these studies, the present data are 35% and 50% slower, respectively. The activation energy between the current data and the ones from Wu et al. is very similar, but the present data are lower by about 35%, despite being measured at slightly higher pressure (k_1 has demonstrated some pressure-dependence in other studies [38,54-56]). It is worth mentioning that the 2 direct measurements of k_1, *i.e.* our study and Kiecherer et al. [56], were obtained with different techniques and yet yield very similar results over the range of temperatures they share (Fig. 9). Note the small discrepancy at lower temperatures between the two studies. This minor discrepancy is most likely due to the scatter induced by the technique used in [56].

In addition, the experimental k_1 value herein is in agreement with some of the theoretical reaction rates found in the literature [54,56]. However, this study has shown high differences with theoretical calculations such as Xu et al. [49] at 1 atm, and the extrapolated calculations of Li et al. [38] at 1.01 bar. Despite finding good agreement between this study and well-known studies in the literature, it is important to indicate that there are still high variations within existing reaction rates in the scientific literature and even seemingly small variations in k_1 can have a great impact on the predictions of the mechanisms, as can be seen by comparing the predictions of the Aramco2.0 model with the predictions of the same model with the present value of k_1 (Figs. 5 and 8).

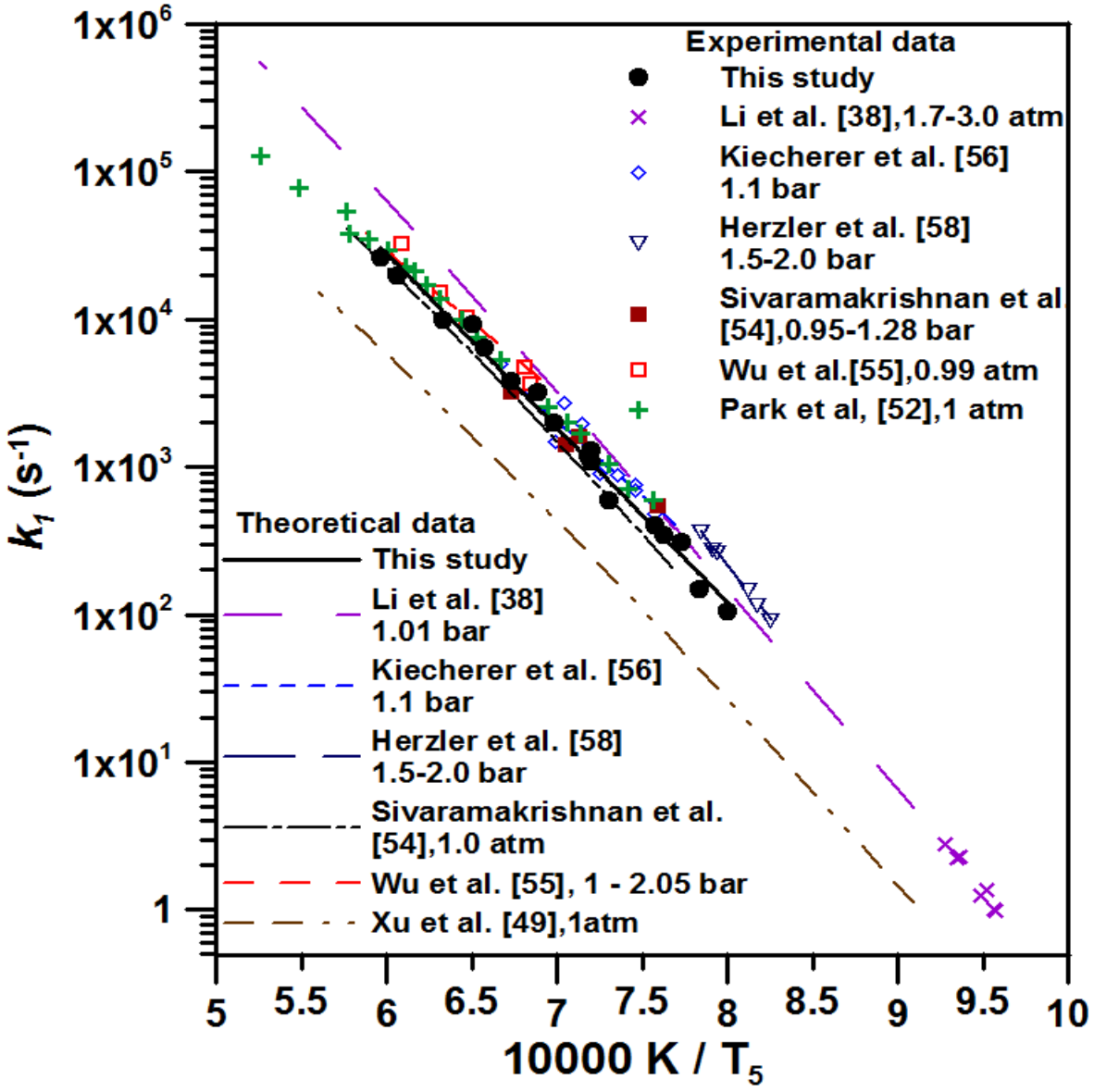

Figure 12: Arrhenius plot of literature studies compared to this study. Symbols represent the experimental data, lines represent theoretical values.

A key issue with R1 is associated with its high-pressure dependency [38,54,56], and it visible that the pressure dependence varies greatly between two studies. For example, the value of k/k_∞ at 1450 K, with k determined at 1 atm, is 1.65 times higher for Sivaramakrishnan et al. [54] than for

Li et al. [38]. These differences are discussed in detail in [54]. More data at higher and lower pressures would be necessary to characterize experimentally the pressure behavior of k_1 and confirm the theoretical calculations. However, since the rate coefficient for k_1 determined herein is in good agreement with the one determined with another technique in [56], we can assume that this value of k_1 can be taken as a reference for the conditions investigated herein. It is visible in Fig. 12 that our rate constant is very close to the one proposed by Sivaramakrishnan et al. [54] (note that the rate coefficient of k_1 for [54] is plotted for a slightly lower pressure of 1 atm). We therefore believe that the pressure dependence described in [54] should be adopted in modern mechanisms, but with a slight adjustment in the rate coefficient to take into account the slight difference observed for k_1 from Sivaramakrishnan et al. [54] and the rate proposed herein (which is, again, in agreement with the measurements of Kiecherer et al. [56]).

4.4 Effect of the Calculated k_1 on Oxidation Condition

The comparison between the pyrolysis data and the predictions of the Aramco 2.0 model with the reaction rate coefficient for k_1 determined herein is visible in Fig. 5. Concerning the oxidation results, it is worth noting that the experimental profiles show a growth in the water concentration in two stages (Figs. 13-15 and additional comparisons are in the Appendix section). The first stage starts very rapidly, at time zero, and can lead to a pseudo-plateau for the lowest temperatures investigated. This first stage essentially corresponds to the rapid formation of water from ethanol thermal dissociation via the reaction k_1, described above. The amount of water produced by this first stage is relatively modest compared to the second stage. The second stage starts more or less rapidly after the first stage, depending on the temperature. As mentioned, for the lowest

temperatures investigated, a plateau in the water concentration can almost be observed between these two growth sequences for H_2O concentration. At high temperature, the second stage can even start immediately after the first stage, resulting in a profile where these two phases are hardly discernable. The amount of water formed during this second stage is large and seems to reach an equilibrium value when the experimental time allows.

These experimental profiles were subsequently modeled with the following detailed kinetics mechanisms: Aramco 2.0, Cancino et al, CRECK, LLNL, and a modified version of Aramco 2.0 which utilizes the rate coefficient of k_1 calculated herein. During this study, as can be seen in Fig. 13, the detailed kinetics models poorly predict the water profiles for the fuel lean case ($\phi = 0.5$) at low temperatures. It was observed that the model from Cancino et al. tends to under-estimate the amount of water during the time period considered, whereas the LLNL mechanism is significantly too reactive and over-estimates the amount of water during the first 1500 μs. The first growth period is well captured by the Aramco 2.0 model, but this model also lacks reactivity at later times, for the second growth. Under this condition, it was observed that the CRECK model was able to give better predictions. Finally, note that the modified version of Aramco 2.0 gives better predictions than the original Aramco 2.0, especially the reactivity of the second period of water formation. At higher temperature, Fig. 13b, the original Aramco 2.0 offers good predictions of the water formation, and the modified Aramco is still able to provide slightly better predictions. Note that the final amount of water is a little over-estimated by the models which, for times longer than 1250 μs, predict a very similar amount of water. The model from Cancino et al. tends to be closer to the experimental data at high temperature compared to itself for the previous low-temperature example, but is still under-reactive overall. The water formation is also over-estimated for this

model, past 1000 µs, by a larger amount than for the Aramco 2.0 model. Concerning this final amount of water, the CRECK mechanism predicts the highest amount while the LLNL model reproduce very well the experimental value, although the model is still significantly too reactive.

It is interesting to see that all models, except the LLNL one, over-estimate the water formation at the plateau, past the second growth. It is also interesting to notice that all models predict a different value at this second plateau. One can therefore conclude that the equilibrium value for water formation is not reached in the time-scale of our experiments. This observation is confirmed by the slowly ascending trend of the water signal, as visible at high temperature. Hence, in addition to the timing of water formation, the level of water reached on the second growth period are very useful data to further refine detailed kinetics mechanisms.

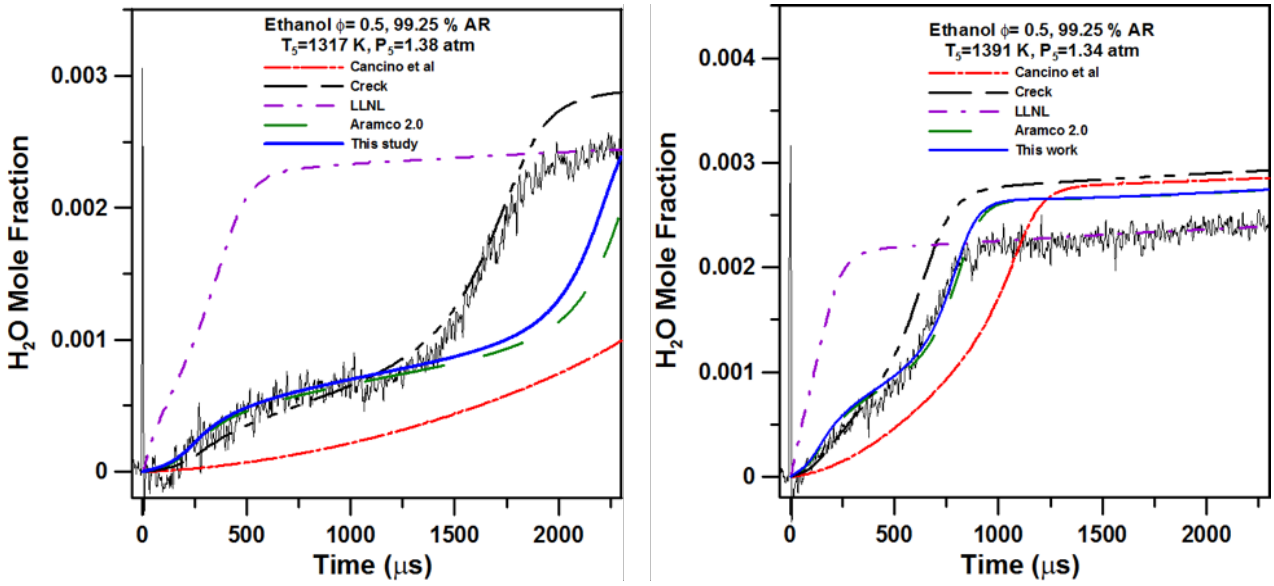

Figure 13: H_2O time-history profiles for the oxidation of ethanol at Φ = 0.5 in 0.9925 Ar and comparison with detailed kinetics models from the literature including rate coefficient from this study.

For the stoichiometric case, Fig. 14, the two versions of the Aramco 2.0 mechanism and the Cancino models present good predictions for low temperatures, except for the first growth with the Cancino et al. model. Note that the amount of water at the second plateau, past 1400 μs, is accurately reproduced by the Aramco 2.0 model. The modified Aramco 2.0 model offers comparable predictions although it is slightly closer to the data. A similar feature can be observed at higher temperature. The CRECK and, to a larger extent, LLNL models are too reactive. However, the final amount of water at the end of the test time is largely over-estimated by the CRECK model.

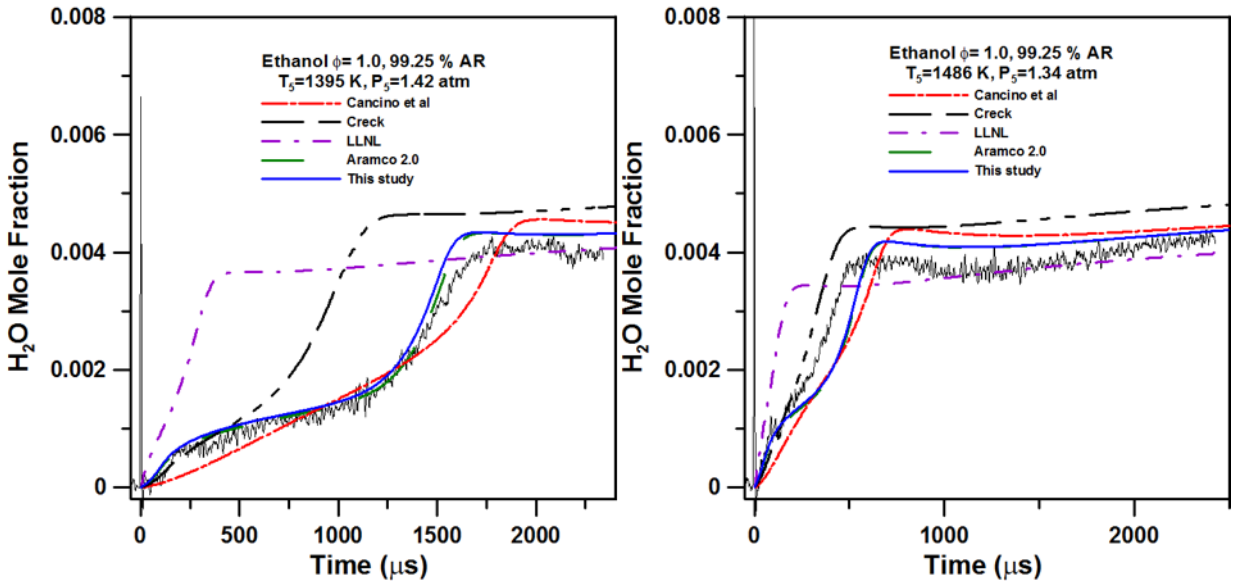

Figure 14: H_2O time-history profiles for the oxidation of ethanol at Φ = 1.0 in 0.9925 Ar and comparison with detailed kinetics models from the literature including rate coefficient from this study.

For Ethanol ϕ = 2.0, Fig. 15, both versions of the Aramco 2.0 model give remarkably accurate predictions of the amount of water at all times. The trend observed for the other models at lower equivalence ratios is carried over this condition. This favorable prediction by Aramco 2.0 shows

that both versions of the Aramco kinetic model have better capabilities for predicting the amount of water for a fuel rich mixture of ethanol highly diluted in Ar, for the range of temperatures investigated herein.

Overall, the present oxidation data show that the modified Aramco 2.0 provides the best predictions of water formation for all three equivalence ratios investigated, under the studied conditions. Moreover, it was observed that better predictions are obtained when the equivalence ratio increases.

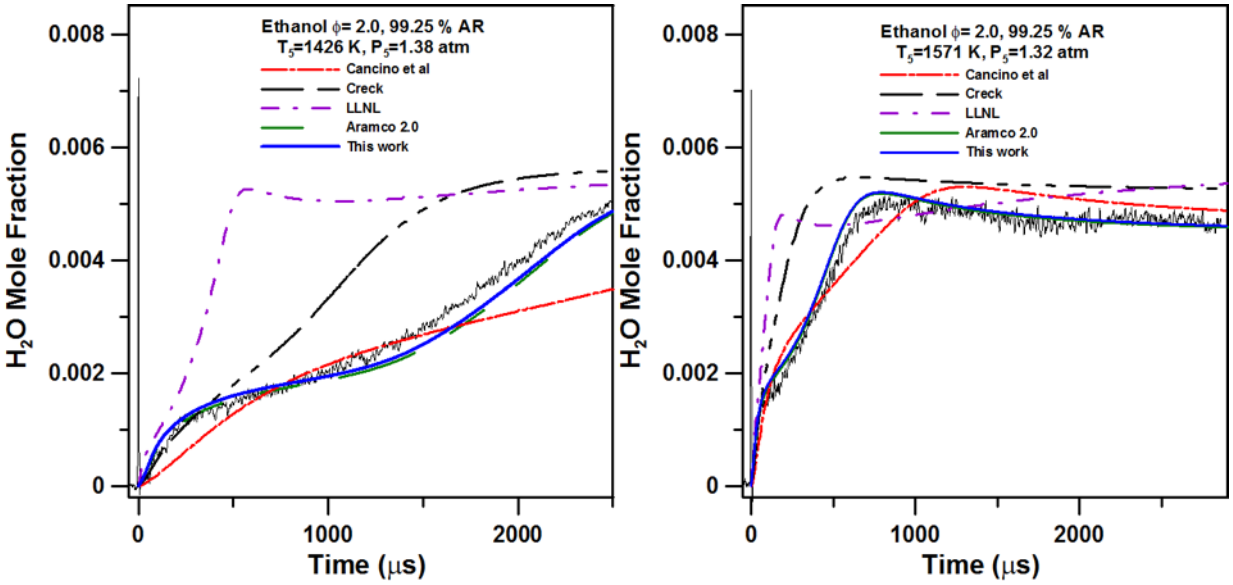

Figure 15: H_2O time-history profiles for the oxidation of ethanol at Φ = 2.0 in 0.9925 Ar and comparison with detailed kinetics models from the literature including rate coefficient from this study.

When adding the reaction rate for k_1 determined herein into the Aramco 2.0 mechanism, one can see some slight improvements in the predictions. The H_2O profiles with Φ = 0.5 in Figure 13 shows

that for the low-temperature experiments, the modified Aramco 2.0 model gives better predictions of the water formation than Aramco 2.0 itself. Especially for later times, after approximately 1250 μs, the modified Aramco 2.0 seems to be more reactive and therefore gives slightly better predictions. For higher temperatures, the same behavior was observed for early times, and for later times the water formation was over-estimated.

Water measurements at $\Phi = 1.0$ consistently show good predictions of the original kinetic mechanism Aramco 2.0 as well as the modified model. For early times, the modified model with this study's rate coefficient gives better predictions of the water formation. For later times, it was observed that both models predict the water formation very similarly, and as the temperature is increased, the models tend to over predict the water formation. Water measurements at $\Phi = 2.0$ were more accurate. Also, better predictions were again obtained with the modified Aramco 2.0.

5. CONCLUSION

Water time-histories were followed from a pyrolytic mixture of ethanol highly diluted in Ar using a laser absorption technique to monitor H_2O concentration behind reflected shock waves. A direct measurement of the reaction coefficient of R1, $C_2H_5OH \leftrightarrows C_2H_4 + H_2O$, was possible at the early moments of the observation time. The value of k_1 determined herein (k_1 (s^{-1}) = $3.37\times10^{11}\exp(-27174\ K/T)$) was found to be in very good agreement with the recent study of Kiecherer et al. [56]. These two studies are the only studies were R1 was directly measured, and the results, obtained on different shock tubes and with different techniques, therefore confirm the rate coefficient of k_1 at around 1 atm presented in this paper. The laser absorption technique employed herein allowed for a smaller scatter in the determination of the rate coefficient of k_1, hence lowering the uncertainty in this reaction rate (determined to be within 20%).

Water time-histories under oxidation conditions highly diluted in Ar show that overall, the modified Aramco 2.0 provides the best predictions of water formation for all three equivalence ratios investigated, and it was observed that better predictions are obtained when the equivalence ratio increases. The present work illustrates the quality of the measurements carried out in the author's laboratory. Noticeable improvements in the predictions of the state-of-the-art detailed kinetics mechanism were brought by measuring the reaction rate coefficient of the thermal decomposition of ethanol. However, this reaction is pressure dependent, and more measurements at higher and lower pressures would be needed to validate further this reaction, especially under conditions that are more practical for combustion devices such as internal combustion engines.

REFERENCES

[1] International Energy Agency. World energy outlook 2012, renewable energy outlook; 2013. Available at: https://www.iea.org/Textbase/npsum/WEO2013SUM.pdf

[2] M. Balat, H. Balat, Appl. Energy 86 (2009) 2273–2282.

[3] R. C. O. B. Delgado, A. S. Araujo, V. J. Fernandes Jr, Fuel Process. Technol. 88 (2007) 365-368.

[4] S. Mani Sarathy, Patrick Oßwald, Nils Hansen, Katharina Kohse-Höinghaus. Progress in Energy and Combustion Science 44 (2014) 40-102.

[5] A. Demirbas. Prog Energy Combust Sci 33 (2007) 1-18.

[6] A.K. Agarwal. Biofuels (alcohols and biodiesel) applications as fuels for internal combustion engines. Prog Energy Combust Sci 33 (2007) 233-271.

[7] H.R Ricardo. The high-speed internal-combustion engine. London Glasgow: Blackie Son Ltd; 1931.

[8] A. Amer, H. Babiker, J. Chang, G. Kalghatgi, P. Adomeit, A. Brassat, et al. SAE Int J Fuels Lubr 5 (2012) 1048-1065.

[9] D. Turner, H. Xu, R. F. Cracknell, V. Natarajan, X. Chen, Fuel 90 (2011) 1999–2006.

[10] K. Kohse-Hoïnghaus, P. Oßwald, T. A. Cool, T. Kasper, N. Hansen, F. Qi, C. K. Westbrook, P. R. Westmoreland, Angew. Chem. 122 (2010) 3652–3679.

[11] D.F. Cooke, M.G.Dodson, A. Williams. Combust Flame 16 (1971) 233-236.

[12] D. Lee, Hochgreb, J.C. Keck. SAE Technical paper 932755 (1993) 1-8.

[13] H. J. Curran, M. P. Dunphy, J. M. Simmie, C. K. Westbrook, W. J. Pitz, Proc. Symp. Combust. 24 (1992), 769−776.

[14] K. A. Heufer, H. Olivier, Shock Waves 20 (2010) 307−316.

[15] L. R. Cancino, M. Fikri, A. A. M. Oliveira, C. Schulz, Energy Fuels 24 (2010) 2830−2840.

[16] E.K. Noorani, B. Akih-Kumgeh, J. M. Bergthorson. Energy Fuels 24 (2010) 5834-5843

[17] C. Lee, S. Vranckx, K. A. Heufer, S. V. Khomik, Y. Uygun, H. Olivier, et al. Z Phys Chem 226 (2012) 1-28.

[18] G. Mittal, S. M. Burke, V. A. Davies, B. Parajuli, W. K. Metcalfe, H. J. Curran. Combust Flame 161 (2014) 1164-1171.

[19] C. L. Barraza-Botet, S. W. Wagnon, M. S. Wooldridge, J. Phys. Chem. A 2016, 120, 7408−7418.

[20] Ö. L. Gülder. Proc Combust Inst 19 (1982) 275 281.

[21] M. Metghalchi, J. C. Keck. Combust Flame 48 (1982) 191-210.

[22] D. Bradley, M. Lawes, M. S. Mansour. Combust Flame 156 (2009) 1462-1470.

[23] P. S. Veloo, Y. L. Wang, F. N. Egolfopoulos, C. K. Westbrook. Combust. Flame 157 (2010) 1989–2004.

[24] J. P. J. van Lipzig, E. J. K. Nilsson, L. P. H. de Goey, A. A. Konnov, Fuel 90 (2011) 2773–2781.

[25] L. Sileghem, V. A. Alekseev, J. Vancoillie, E. J. K. Nilsson, S. Verhelst, A. A. Konnov, Fuel 115 (2014) 32–40.

[26] P. Dirrenberger, P. A. Glaude, R. Bounaceur, H. Le Gall, A. Pires da Cruz, A. A. Konnov, F. Battin-Leclerc, Fuel 115 (2014) 162–169.

[27] T Knorsch, A. Zackel, D. Mamaikin, L. Zigan, M. Wensing. Energy Fuels 28 (2014) 1446-1452.

[28] M. Aghsaee, D. Nativel, M. Bozkurt, M. Fikri, N. Chaumeix, C. Schulz. Proceed. Combust. Instit. 35 (2015) 393–400.

[29] A. A. Konnov, R.J. Meuwissen, L.P.H. de Goey, Proc. Combust. Inst. 33 (2011) 1011–1019.

[30] S. Y. Liao, D. M. Jiang, Z. H. Huang, K. Zeng. Appl Therm Eng 27 (2007) 374-380.

[31] J. Beeckmann, L. Cai, H. Pitsch. Fuel 117 (2014) 340-350

[32] J. P. J. van Lipzig, E. J. K. Nilsson, L. P. H. de Goey, A. A. Konnov, Fuel 90 (2011) 2773–2781.

[33] T. S. Norton, F. L. Dryer. Proc Combust Inst 23 (1991) 179-185.

[34] G. Rotzoll. J Anal Appl Pyrolysis 9 (1985) 43-52.

[35] T. S. Norton, F. L. Dryer FL. Int J Chem Kinet 24 (1992) 319-344.

[36] J. Li, A. Kazakov, F. L. Dryer. Int J Chem Kinet 33 (2001) 859-867.

[37] M. U. Alzueta, J. M. Hernández. Energy Fuels 16 (2002) 166-171.

[38] J. Li, A. Kazakov, F. L. Dryer, J. Phys. Chem. A 108 (2004) 7671−7680.

[39] F. Herrmann, B. Jochim, P. Oßwald, L. Cai, H. Pitsch, K. Kohse-Höinghaus. Combust Flame 116 (2014) 384-397.

[40] P. Dagaut, J. C, Boettner, M. Cathonnet. J Chim Phys Pcb 89 (1992) 867-884.

[41] P. Dagaut, C. Togbé. Energy Fuels 22 (2008) 3499-3505.

[42] N. Leplat, P. Dagaut, C. Togbé, J. Vandooren. Combust Flame 158 (2011) 705-725.

[43] Y. Hidaka, H. Wakamatsu, M. Moriyama, T. Koike, K. Yasunaga. In: Shock Waves. Berlin Heidelberg: Springer; 2005: 651-656.

[44] H. Nakamura, A. Yamamoto, M. Hori, T. Tezuka, S. Hasegawa, K. Maruta. Proc. Comb. Inst. 34 (2013) 3435–3443

[45] L. H. Benvenutti, C. S. T. Marques, C. A. Bertran. Combust Sci Technol 177 (2004) 1-26.

[46] A. Ergut, S. Granata, J. Jordan, J. Carlson, J. B. Howard, H. Richter, et al. Combust Flame 144 (2006) 757-772.

[47] T. S. Kasper, P. Oßwald, M. Kamphus, K. Kohse-Höinghaus. Combust Flame 150 (2007) 220-231.

[48] P. Saxena P, F. A. Williams. Proc Combust Inst 31 (2007) 1149-1156.

[49] H. Xu, C. Yao, T. Yuan, K. Zhang, H. Guo. Combust Flame 158 (2011) 1673-1681.

[50] L.-S. Tran, P.-A. Glaude, R. Fournet, F. Battin-Leclerc. Energy Fuels 27 (2013) 2226-2245.

[51] M. N. Marinov, Int. J. Chem. Kinet. 31 (1999) 183-220.

[52] J. Park, R. S. Zhu, M. C. Lin, J. Chem. Phys. 117 (2002) 3224-3231.

[53] W. Tsang, Int. J. Chem. Kinet. 36 (2004) 456-465.

[54] R. Sivaramakrishnan, M.-C. Su, J. V. Michael, S. J. Klippenstein, L. B. Harding, B. Ruscic, J. Phys. Chem. A. 114 9425-9439.

[55] C.-W. Wu, H. Matsui, N.-S. Wang, M. C. Lin, J Chem. Phys. A 115 (2011) 8086-8092.

[56] J. Kiecherer, C. Bansch, T. Bentz, M. Olzmann, Proceed. Combust. Instit. 35 (2015) 465-472.

[57] N. I. Butkovskaya, Y. Zhao, D. W. Setser, J. Phys. Chem. 98 (1994) 10779–10786.

[58] J. Herzler, J. A. Manion, W. Tsang, J. Phys. Chem. A 101 (1997) 5500–5508.

[59] E. L. Petersen, M. J. A. Rickard, M.W. Crofton, E. D. Abbey, M. J. Traum, D. M. Kalitan, Meas. Sci. Technol. 16 (2005) 1716-1729.

[60] CHEMKIN-PRO 18.0, Ansys, 2018.

[61] L. S. Rothman, D. Jacquemart, A. Barbe, D. Chris Benner, M. Birk, L. R. Brown, M. R. Carleer, C. Chackerian Jr., K. Chance, L. H. Coudert, et al.Journal of Quantitative Spectroscopy and Radiative Transfer 96 (2005) 139-204.

[62] E. E. Whiting. Journal of Quantitative Spectroscopy & Radiative Transfer 8 (1968) 1379-1384.

[63] V. Nagali, D. F. Davidson, R. K. Hanson, Journal of Quantitative Spectroscopy & Radiative Transfer 64 (2000) 651-655.

[64] O. Mathieu, C. Mulvihill, E. L. Petersen, Proc. Comb. Inst. 36 (2017) 4019-4027.

[65] Available at https://www.ems.psu.edu/~radovic/ChemKin_Theory_PaSR.pdf PaSR.pdf

[66] M. Mehl , W. J. Pitz, C. K. Westbrook, H. J. Curran, Proceed. Combust. Instit. 33 (2011) 193-200.

[67] E. Ranzi, A. Frassoldati, R. Grana, A. Cuoci, T. Faravelli, A. P. Kelley, C. K. Law, Progress Energy Combust. Sci. 38 (2012) 468-501.

[68] C1-C3 mechanism (Version 1412, December 2014) available for download at: http://creckmodeling.chem.polimi.it/menu-kinetics/menu-kinetics-detailed-mechanisms/menu kinetics-c1-c3-mechanism (Last consulted on 11/2016) 6/2017).

[69] Aramcomech 2.0 available for download at: http://www.nuigalway.ie/c3/aramco2/frontmatter.html (last consulted on 11/2016)

[70] J. P. Senosiain, S. J. Klippenstein, J. A. Miller, J. Phys. Chem. A 110 (2006) 6960-6970

[71] J. E. Vivanco (2014). A new shock tube facility for the study of high-temperature chemical kinetis. Master's thesis, Texas A& M Univeristy.Available electronically from http://hdl.handle.net/1969.1/153885

APPENDIX

A. Best k_1 fit

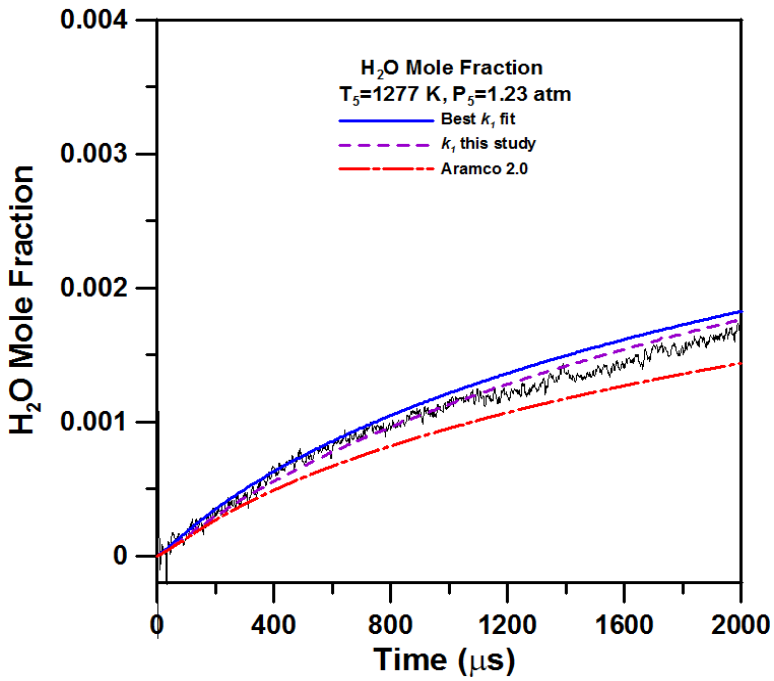

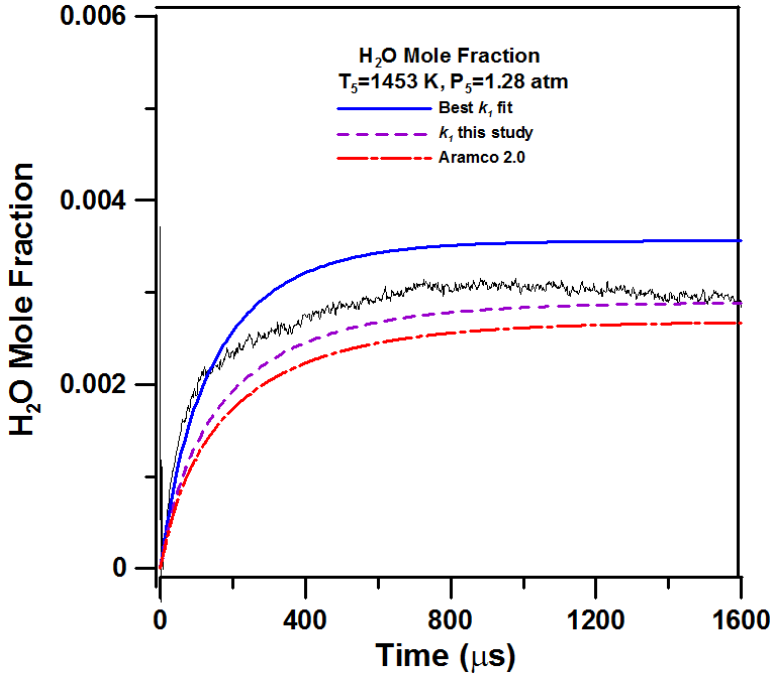

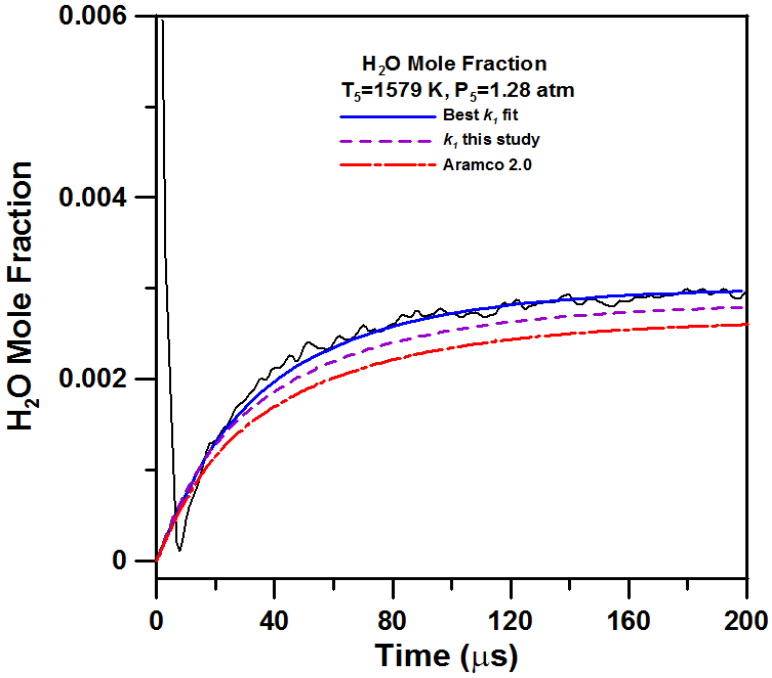
H2O Mole Fraction
T5=1579 K, P5=1.28 atm
Best k1 fit
k1 this study
Aramco 2.0
H2O Mole Fraction
0.006
0.004
0.002
0
0
40
80
120
160
200
Time (μs)

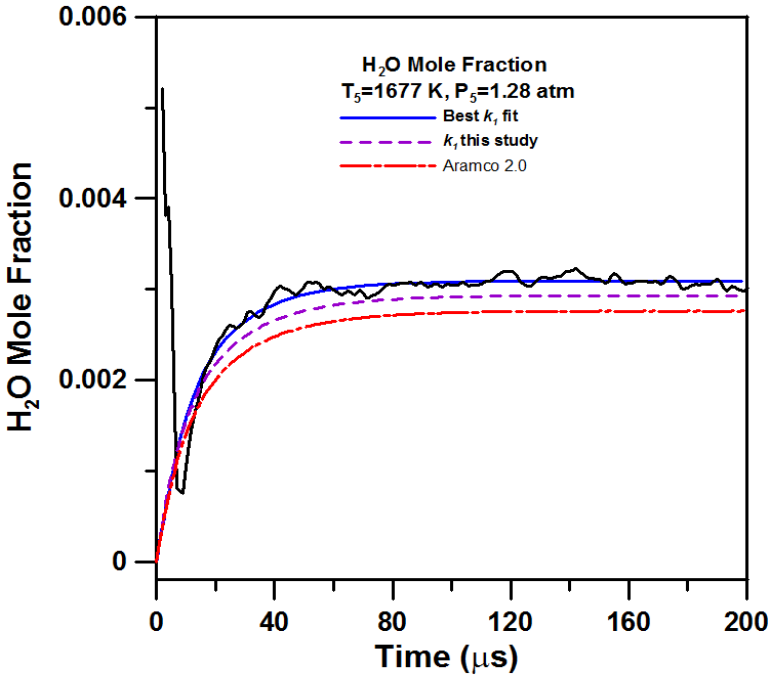
H2O Mole Fraction
T5=1677 K, P5=1.28 atm
Best k1 fit
k1 this study
Aramco 2.0
H2O Mole Fraction
0.006
0.004
0.002
0
0
40
80
120
160
200
Time (μs)

B. H_2O time-history profiles for the pyrolysis of ethanol

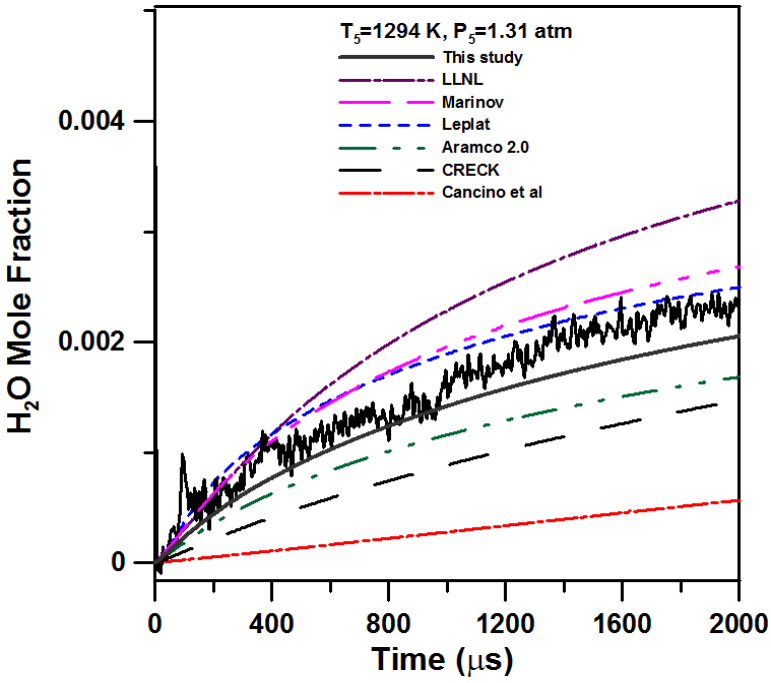

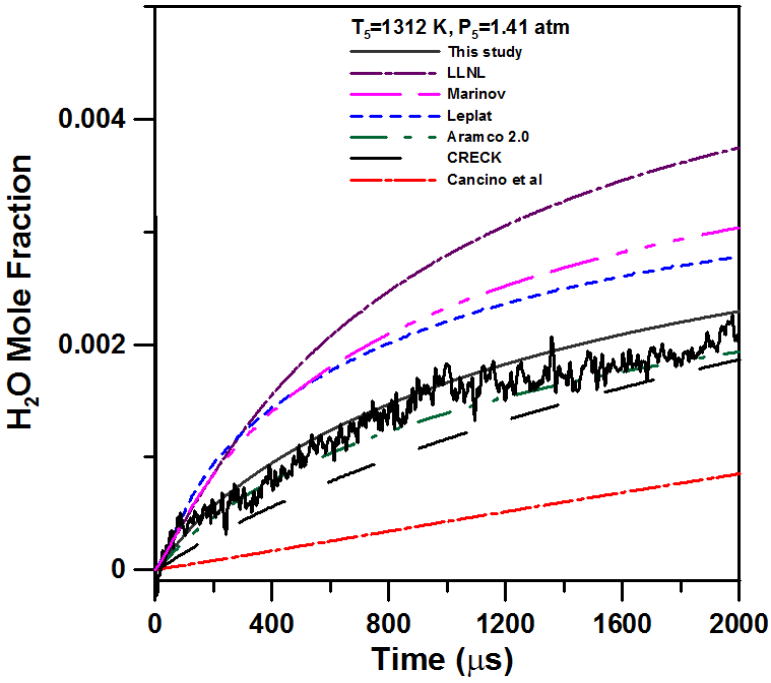

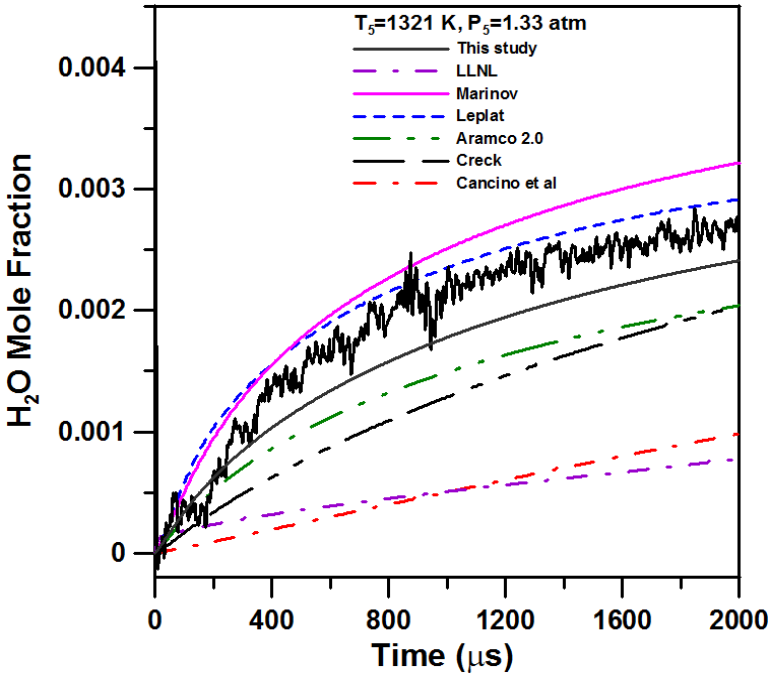
T5=1321 K, P5=1.33 atm
This study
LLNL
Marinov
Leplat
Aramco 2.0
Creck
Cancino et al
H2O Mole Fraction
0.004
0.003
0.002
0.001
0
0
400
800
1200
1600
2000
Time (μs)

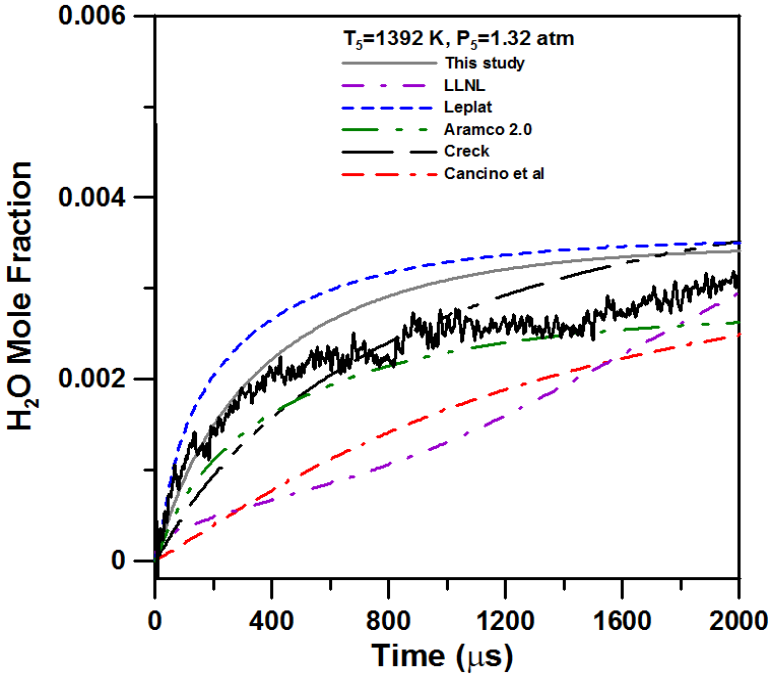
T5=1392 K, P5=1.32 atm
This study
LLNL
Leplat
Aramco 2.0
Creck
Cancino et al
H2O Mole Fraction
0.006
0.004
0.002
0
0
400
800
1200
1600
2000
Time (μs)

C. H_2O time-history profiles for the oxidation of ethanol at Φ=0.5

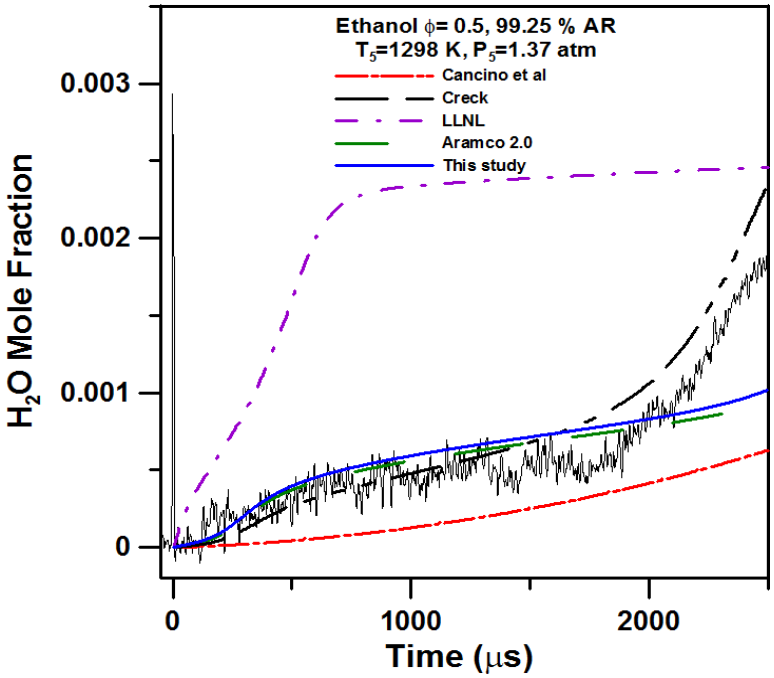

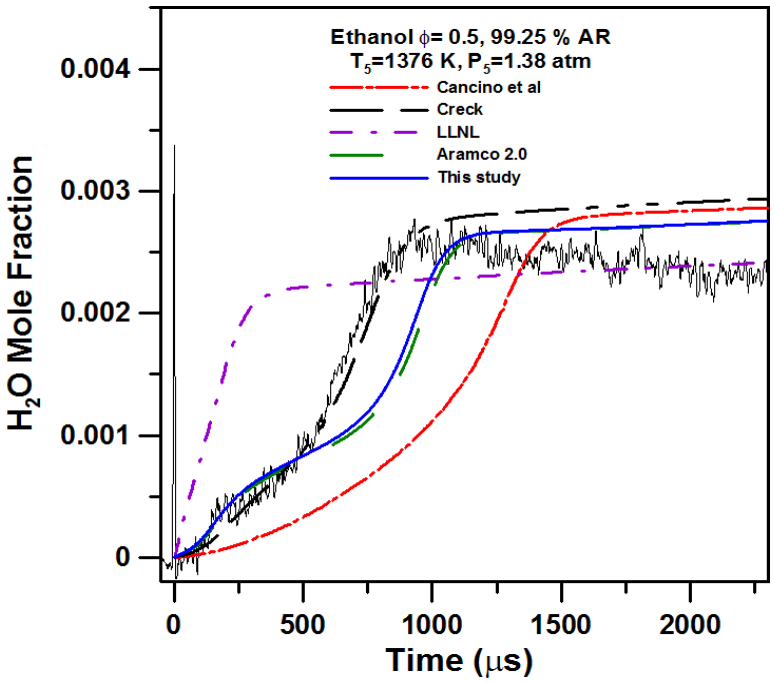

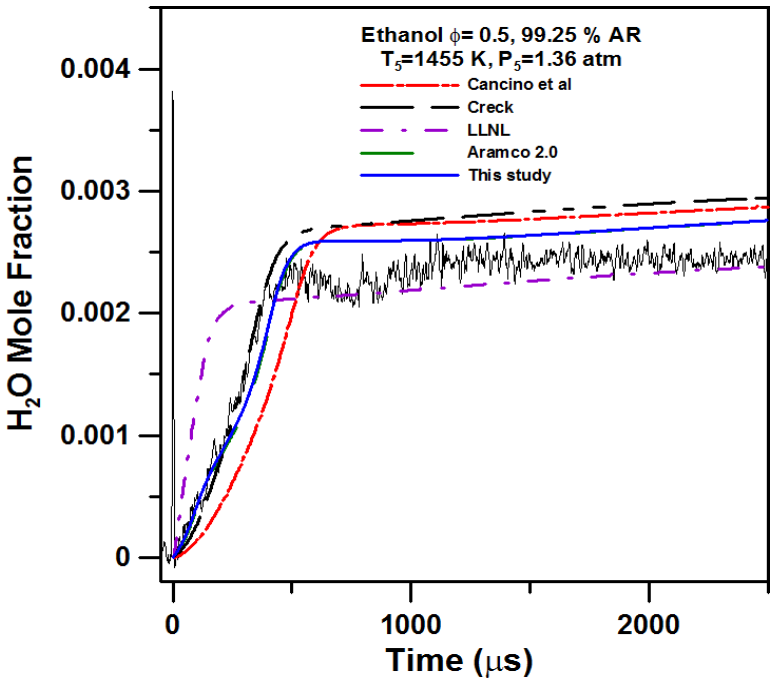
Ethanol ϕ= 0.5, 99.25 % AR
T5=1455 K, P5=1.36 atm
Cancino et al
Creck
LLNL
Aramco 2.0
This study
H2O Mole Fraction
0.004
0.003
0.002
0.001
0
0
1000
2000
Time (μs)

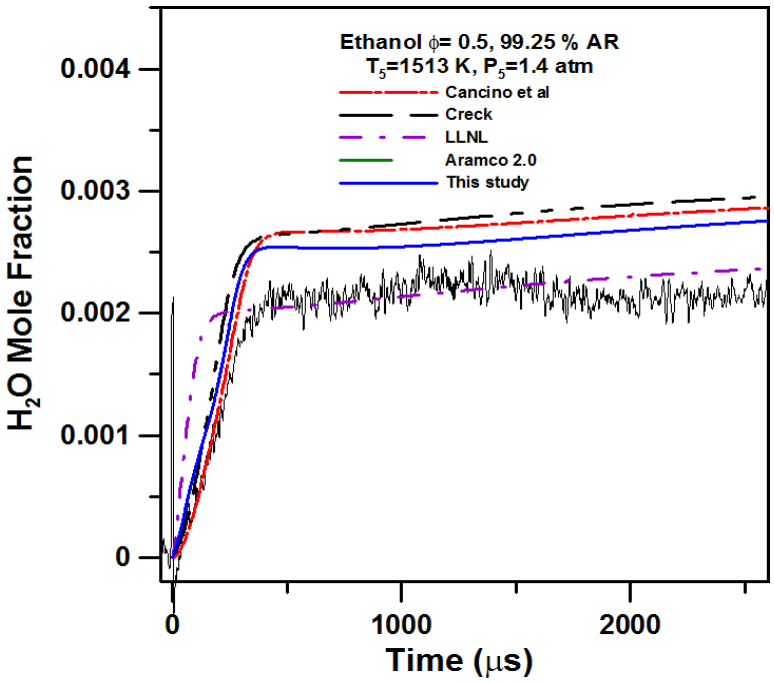
Ethanol ϕ= 0.5, 99.25 % AR
T5=1513 K, P5=1.4 atm
Cancino et al
Creck
LLNL
Aramco 2.0
This study
H2O Mole Fraction
0.004
0.003
0.002
0.001
0
0
1000
2000
Time (μs)

D. H_2O time-history profiles for the oxidation of ethanol at Φ=1.0

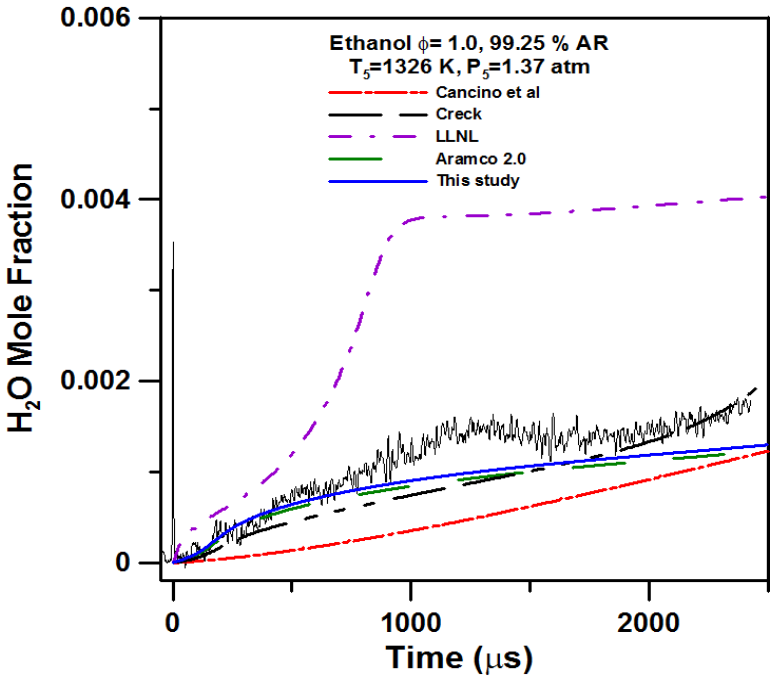

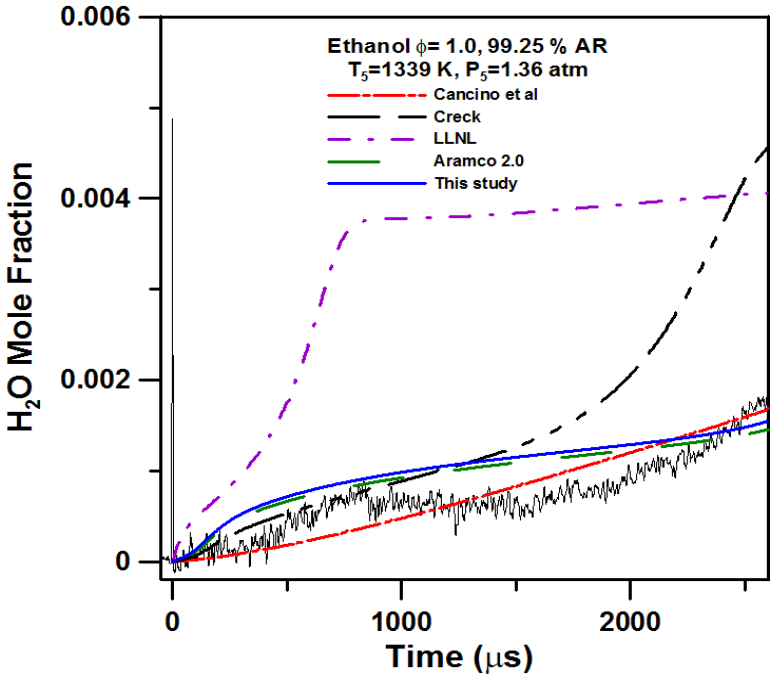

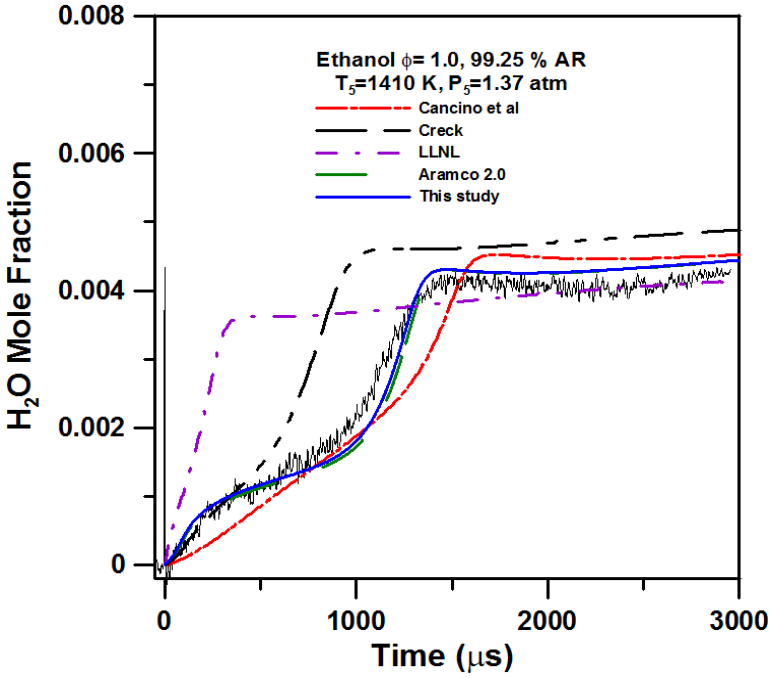
Ethanol ϕ= 1.0, 99.25 % AR
T5=1410 K, P5=1.37 atm
Cancino et al
Creck
LLNL
Aramco 2.0
This study
H2O Mole Fraction
Time (μs)
0.008
0.006
0.004
0.002
0
0
1000
2000
3000

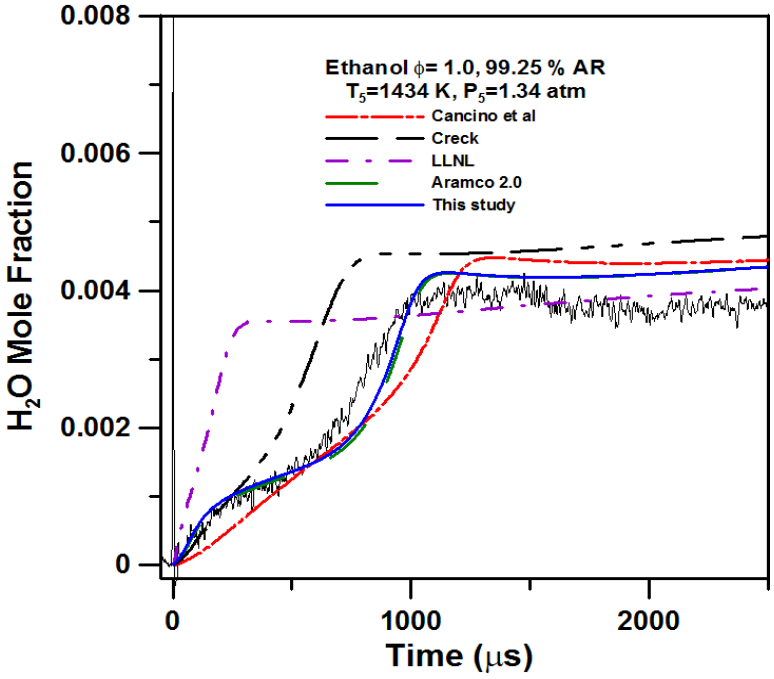
Ethanol ϕ= 1.0, 99.25 % AR
T5=1434 K, P5=1.34 atm
Cancino et al
Creck
LLNL
Aramco 2.0
This study
H2O Mole Fraction
Time (μs)
0.008
0.006
0.004
0.002
0
0
1000
2000

E. H_2O time-history profiles for the oxidation of ethanol at Φ=2.0

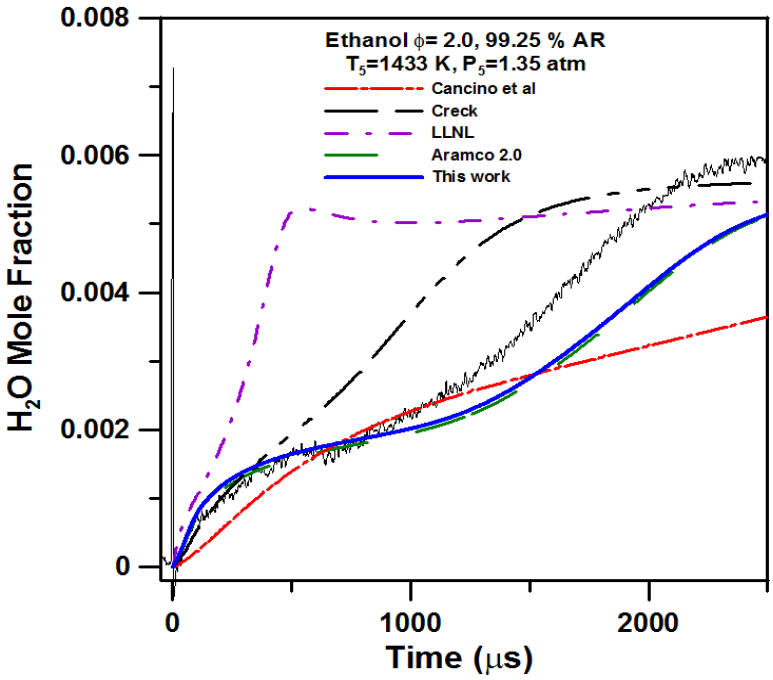

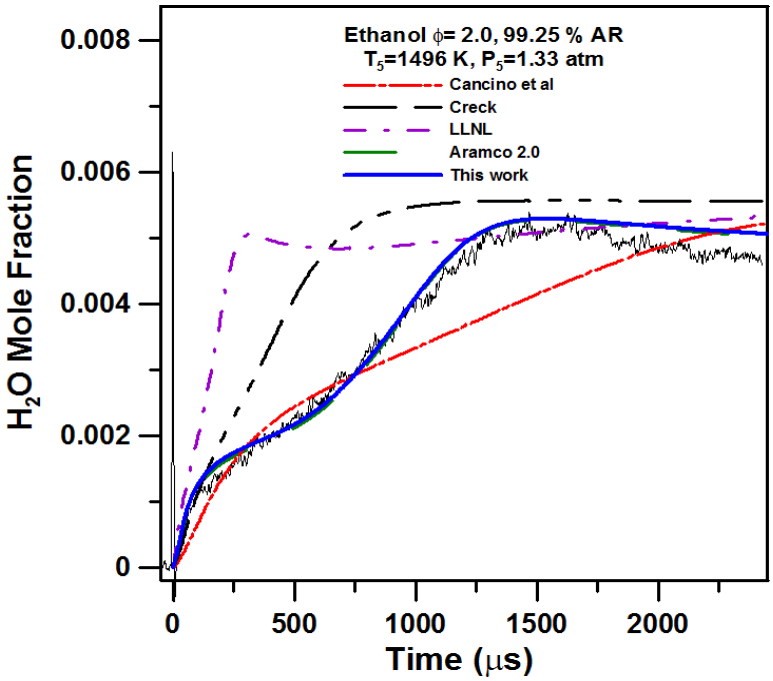

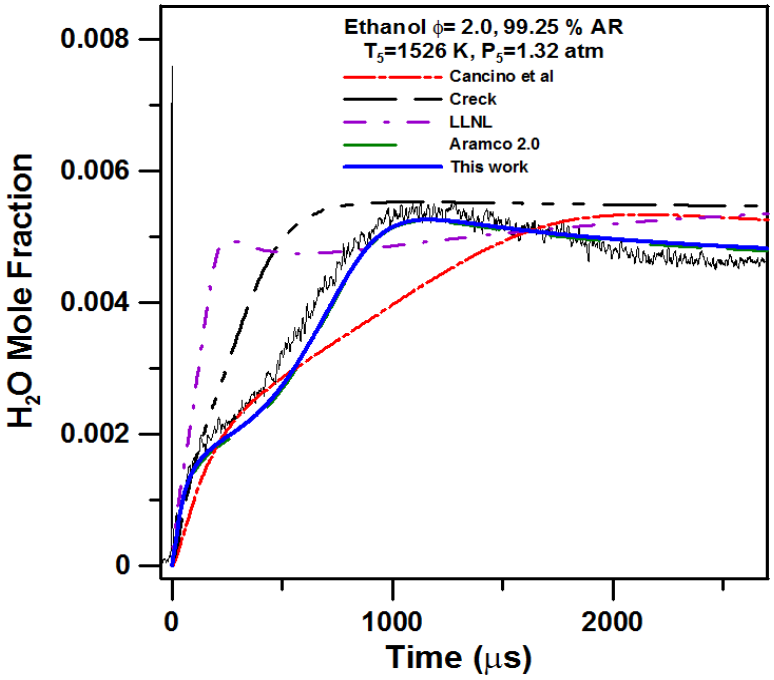
Ethanol ϕ= 2.0, 99.25 % AR
T5=1526 K, P5=1.32 atm
Cancino et al
Creck
LLNL
Aramco 2.0
This work
H2O Mole Fraction
0.008
0.006
0.004
0.002
0
0
1000
2000
Time (μs)

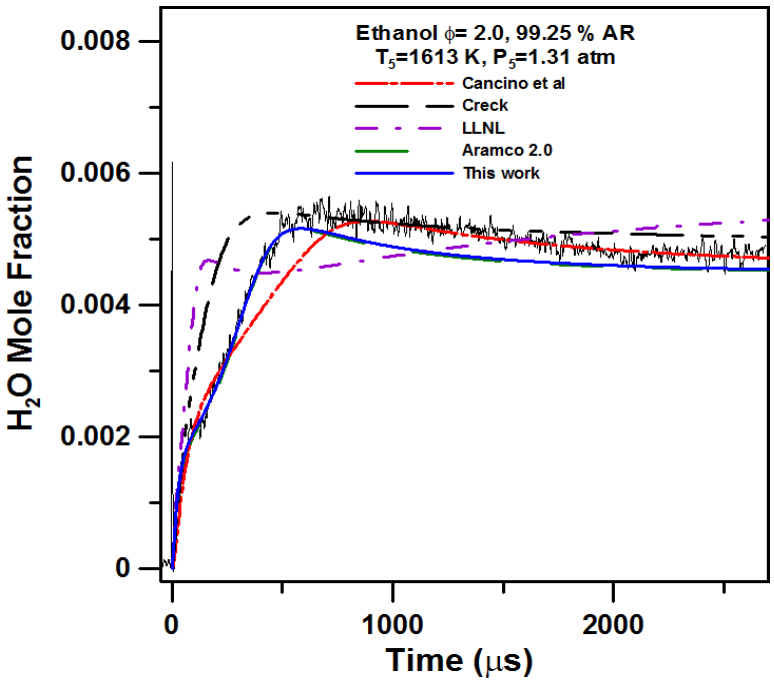
Ethanol ϕ= 2.0, 99.25 % AR
T5=1613 K, P5=1.31 atm
Cancino et al
Creck
LLNL
Aramco 2.0
This work
H2O Mole Fraction
0.008
0.006
0.004
0.002
0
0
1000
2000
Time (μs)